

# Fractal analysis of geomagnetic data to decipher pre-earthquake process in Andaman-Nicobar region, India

Rahul Prajapati<sup>1\*</sup> and Kusumita Arora <sup>1</sup>

<sup>1</sup> Geomagnetism Group, CSIR-National Geophysical Research Institute, Hyderabad-500007, India; rahulphy007@gmail.com

\*Correspondence: [rahulphy007@gmail.com](mailto:rahulphy007@gmail.com)

**Abstract:** Seismo-electromagnetic (SEM) signatures recorded in geomagnetic data, prior to earthquake, has the potential to reveal pre-earthquake processes in focal zones. The present study analyses the vertical component of geomagnetic field data from Mar 2019 to Apr 2020 using fractal and multifractal approach to identify the EM signatures in Campbell Bay (CBY), a seismically active region of Andaman and Nicobar. The significant enhancements in monofractal dimension and spectrum width components of multifractal analysis arise due to superposition high and low frequency SEM emitted from the pre-earthquake processes. It is observed that the higher frequency components, associated with microfracturing dominate signatures of earthquakes occurring around the West Andaman Fault (WAF) and Andaman Trench (AT), while the lower frequencies, which results from slower electrokinetic mechanisms have some correlation with the earthquakes around the Seulimeum Strand (SS) fault. Thus, the mono fractal, spectrum width, and holder exponent parameter reveals different nature of pre-earthquake processes which can be identified on an average of 10, 12, and 20 days prior to the moderate earthquakes within a radius of 60 km, which holds promise of short -term earthquake prediction.

**Keywords:** Geomagnetic; earthquake precursor; Fractal; Andaman-Nicobar

## 1. Introduction

The existence of precursory signatures prior to an earthquake is a hotly debated topic among researchers across the globe. Several convincing evidences of gas exhalations, variations in groundwater level, temperature variations, fluctuations in the electric and magnetic fields, etc., (Scholz et al., 1973; Rikitake, 1975; Crampin et al., 1980; Bella et al., 1995; Virk et al., 2001; Chadha et al., 2008; Koizumi et al., 2004; Liu et al., 2006; Ouzounov et al., 2007; Panda et al., 1996, 2007; Sethumadhav et al., 2010; Hayakawa and Molchanov, 2004), tilts the scale in favor of detectable signatures of pre-earthquake phenomena. Heterogeneous lithospheric material under strain undergoes micro-fracturing, which causes the polarization of charges, which in turn leads to generation of electromagnetic emission and acousto-gravity waves (Molchanov and Hayakawa, 1995). It has been postulated that most crustal rocks contain dormant electronic charge carriers in the form of peroxy defects, which are released under critical stress levels and flow out of the stressed sub volume as an electric current, which generates magnetic field variations and low frequency EM emissions (Freund and Sornette, 2007). When they reach the Earth's surface, they lead to ionization of air at the ground-air interface (Hayakawa et al., 1996), leading to small disturbances in the local geomagnetic field. Observations of electromagnetic emissions prior to earthquake in frequency ranges from DC, ultra-low frequency, very low frequency, electromagnetic pulses, and very high frequency (Bulusu et al., 2023; Conti et al., 2021; Han et al., 2016; Hattori et al., 2013a; Hayakawa et al., 1999, 1996; Johnston et al., 1984) have been reported by many researchers. Presence of precursory signatures in the ULF range have been extensively studied for earthquakes of  $M \geq 7$ , such as Biak, Spitak, Loma Prieta, Guam, Chi-Chi, Chiapas etc., (Fraser - Smith et al., 1990; Hattori et al., 2004b; Hayakawa et al., 2000, 1999; Ida et al., 2008; Kopytenko et al., 1993; Molchanov et al., 1992; Smirnova et al., 2013; Stanica and Stănică, 2019; Yen et al., 2004); the ULF range has received more attention as they experience less attenuation and are more likely to reach the Earth's

surface and geomagnetic recording station. Hayakawa et al. (2005) have examined the 3-component data from the same station to identify the anomalous signatures in the polarization ratio of the ULF geomagnetic signal and the diurnal ratio of the Z component for these moderate earthquakes and found a correlatable pattern of these signatures with earthquake occurrence in 75% of the events. This encouraged a deeper investigation into the possible causes of these patterns.

Identification of the geomagnetic anomalies, which are associated with lithospheric processes is a contentious issue. These variations must be uniquely identified, which are distinct from the expressions of magnetospheric-ionospheric processes due to interaction with the solar wind. The most preferred signal processing techniques in previous studies are polarization ratio analysis, diurnal ratio, principal component analysis, singular value decomposition, mono-fractal, and multifractal analysis (Bulusu et al., 2023; Gotoh et al., 2002; Hattori et al., 2004b; Hayakawa et al., 2007, 2005, 1999; Rawat et al., 2016). These signal processing techniques have shown promising results in different cases such as central frequency of 0.01 Hz of non-overlapping window of night time data studied by Han et al. (2015), Hattori et al. (2013b), and Xu et al. (2013), using filtered diurnal signal (using db5 wavelet function) of target station and reference station; Han et al. (2015) have studied diurnal ratio of electric as well as magnetic fields along with polarization ratio of magnetic field of night time data in the ULF range, and Heavlin et al. (2022) studied the signal from a dense network of stations using linear discrimination analysis (LDA) in frequency range 0.001-25 Hz.

The Andaman-Nicobar region lies in the northern part of the Sumatra subduction zone, where the Indian plate is thrusting under the Burma microplate (Gahalaut et al., 2013; Meng et al., 2012; Yang et al., 2017). Persistent tectonic activity is observed here along three major faults, i.e. West Andaman Fault (WAF), Aceh Strands (AS), and Seulimeum Strands (SS). Some of the major earthquakes along these

faults have led to huge losses of life and property and continue to be a worrisome source of mega-scale hazards. During Mar-2019 to Apr-2020, 63 moderate earthquakes of  $M \geq 4.5$  occurred in the vicinity of the geomagnetic station installed by CSIR-NGRI at Campbell Bay (CBY) in Great Nicobar (Figure 1). The property of Self Organized Critically (SOC) of earthquakes provides the motivation to study the fractal characteristics of the geomagnetic time series to decipher the nature of the anomalous signatures in the data (Bak et al., 1988; Hayakawa et al., 1999).

Behavior of natural biological, physical, and geophysical parameters exhibit fractal and multifractal geometries. Mandelbrot (1977, 1982) introduced fractals to characterize the highly complex geometry such as shape of cloud, coastlines, rough surfaces of mountains and landscapes, where traditional Euclidean geometry fails to characterize the nature of such complex geometries, whereas fractals facilitate description of complex geometries (Barnsley et al., 1989). In 1977, after publication of Mandelbrot's book 'Fractals: From, Chance and Dimension', the concept of fractal geometries has been considered as a popular tool among researchers of remote sensing for extraction of land surface features from high resolution remote sense data (Haralick et al. 1973, Weszka et al. 1976, Gong et al. 1992). Several applications of fractals are observed in image processing for decomposition and extraction of image texture (Pentland 1984, Myint 2003). Moreover, the urban system (population size and areas) also shows scaling and SOC nature and the nature of its growth, economics, morphology, genesis and planning well characterize by fractal approach (Keersmaecker et al., 2003; Chen and Zhou, 2008; Chen, 2010). Fractal has diverse application in field of science, such as, medical science (Lopes and Betrouni, 2009), material science (Schafer, 2013), telecommunication (Werner et al., 2002), environmental science (Xu et al., 1993), and computer graphics (Jacquin, 2002). After gaining popularity in space domain, applications of fractal methods on time domain data started in the 1980-s in the field of finance and

economics to characterize rapidly evolving systems. Application of fractals is also observed in 92

geophysical time series data in characterization of natural phenomenon such as solar corona, and space 93

plasmas (Nabulsi and Anukool.,2024; Borovsky, 2021), frequency size distribution of earthquakes or 94

temporal patterns of earthquake parameters such as magnitude, energy, depth, and hypocenter (Hayat et 95

al., 2019; Telesca et al., 2003; Rahimi et al., 2022), and modelling of geological features from 96

geophysical data such as seismology, earthquake dynamics, and well logs etc., (Ahmed et al., 2022; 97

Leary, 1991; Dolan et al., 1988). In recent years, it is noted that, the natural lithospheric processes due 98

tectonic activity such as heat flow on oceanic ridges (Cheng, 2016), mineralization due to hydrothermal 99

(Wang et al., 2017), and earthquakes with different magnitude (Turcotte, [1997](#)) exhibit the fractal nature. 100

From fractal theory, the changes in fractal dimension represent dynamic evolution of the state of the 101

system; the non-linear dynamics of active plate tectonic can be modeled with fractal geometry (Dimri, 102

2005). The fractal method has become a popular tool in characterization the complexity of dynamic 103

evolution of several type of natural processes including complex behavior of seismicity. The fractal 104

nature of distribution of hypocenter and seismicity pattern was first demonstrated by Kagan and Knopff 105

(1980), and Hirata and Imoto (1991). The spatial distribution of earthquakes shows fractal behavior, 106

wherein the fractal dimension can give an idea of heterogeneities of geological compositions and degree 107

of fracturing of rocks (Pasten and Orrego, 2023). Fractal methods such as Hausdorff dimension, box 108

counting, and correlation dimension are commonly used to study the complex nature of the Earth system 109

and extract deeper insights into seismicity and its relation to tectonic forces (Potirakis et al., 2017; 110

Molchan and Kronrod, 2009; Chen et al., 2006; Mandal et al., 2005). The efficacy of applying the fractal 111

methods to study geomagnetic field patterns prior to earthquake occurrence was a later development 112

(Hattori et al., 2004; Potirakis., 2017; Ida et al., 2012; Hayakawa and Itoh., 2000). For example, in the 113

case of the Guam earthquake, 1993, a significant change in scaling exponent prior to the event is found 114  
(Hayakawa et al., 1999). A similar behavior of scaling exponent was also observed prior to the Biak 115  
earthquake in 1996 (Hayakawa et al., 2000). 116

After the several application of fractals in earthquake research, the researcher found that the earthquake 117  
processes and seismicity in time and space are comprises more than one fractal properties i.e. multifractal 118  
instead of fractal. Multifractal methods have diverse applications in extracting the dynamic nature of 119  
earthquakes in both spatial and time domains. In spatial domain, the multifractal analysis used to 120  
characterize the pattern of seismicity, stress distribution, clustering or intermittency of spatial earthquake 121  
distribution (Godano et al., 1996; Roy and Mondal, 2012; Casado et al., 2014, Rossi, 1990). Multifractal 122  
analysis of the dynamic properties of earthquakes in the time domain reveals the temporal complexity 123  
of seismic activity. This insight into earthquake dynamics may aid in forecasting future seismic events. 124

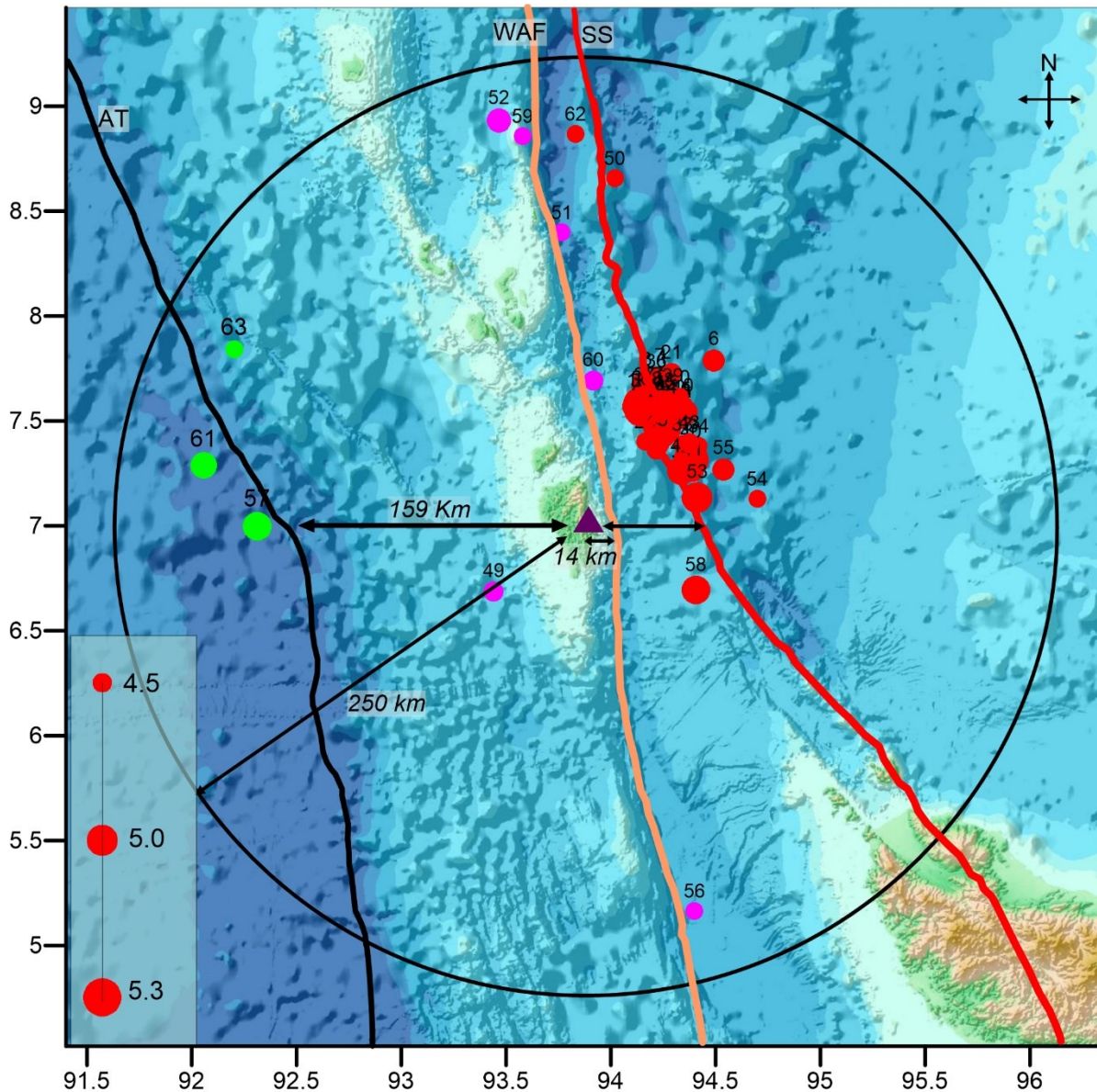
For example, Kiyaschenco et al. (2003) studied the dynamics of seismicity distribution using multifractal 125  
parameters (minimum of holder exponent and first order holder exponent) and found a significant 126  
decrease prior to major earthquakes. Such characteristics can be used as earthquake precursory 127  
signatures. Similarly, Telesca et al. (2004) studied the geomagnetic field from two seismically active 128  
regions (Japan and California) and found that temporal variations in multifractal parameters namely 129  
entropy and higher-order fractal dimensions, which may indicate processes associated with the 130  
preparation of large magnitude earthquakes. Moreover, the generalized multifractal dimension at higher 131  
orders ( $q > 1$ ) of ULF geomagnetic field data showed a significant change prior to the 1993 Guam 132  
earthquake (Ida et al., 2005). Similarly, multifractal analysis of geomagnetic signals from volcanic 133  
eruptions revealed complex dynamics that decreased after eruptions (Currenti et al., 2005). Further, 134  
Telesca et al. (2003) analyzed geoelectrical signals recorded in seismically active regions using fractal 135

and multifractal tools and concluded that the multifractal tools have greater potential for extracting 136  
seismo-electrical signatures associated with earthquakes. Smirnova et al. (2013) observed a notable 137  
decrease in the higher-order fractal dimension (derived from the generalized fractal dimension) of 138  
geomagnetic signals prior to the 1995 Kobe earthquake. 139

These natural non-linear processes give rise to self-similar pattern and long-range correlations, which 140  
are mathematically described by power law relations. Box counting and Hausdorff method are the two 141  
fundamentals methods to determine the fractal dimension of geometries in time or space domain. The 142  
box counting involves the counting of boxes (of fixed sizes) that contains the at least one values of fractal 143  
object (Larry and Toth, 1989). This process is repeated with different box sizes; therefore, the size of 144  
boxes and number of boxes with at least one values relate to the fractal dimension of objects. The 145  
Hausdorff method is similar to box counting, except that the fractal object is visited by different diameter, 146  
and the measured fractal values are called Hausdorff measures. The Hausdorff dimension is related to 147  
the Housdorff measures and the variable diameters used for measure the fractal objects. The fractal 148  
methods such as Detrended Fluctuation Analysis (DFA), scaling structure function, and Higuchi fractal 149  
dimension are common methods for analyzing the geomagnetic signals. Moreover, multifractal 150  
geometries do not exhibit self-similar pattern and holding different fractal dimensions. The spectra of 151  
fractal dimension values determined from sets of fractals used to delineate the multifractal nature of 152  
objects, also known as generalized fractal dimension (Mandelbrot, 1989). In multifractals, the frequency 153  
of exponents or fractal dimension indicates the presence of prominent fractal nature of geometries. The 154  
strength of fractals or their weight are measured by certain parameter  $q$  in the range of  $0 < q > 0$ . The 155  
multifractal methods, Wavelet Transform Modulus Maxima (WTMM) or wavelet Discrete Wavelet 156

Transform (DWT), and Multifractal Detrended Fluctuation Analysis (MFDFA) are very common methods for analysis of geomagnetic signals. For our data, the fractal nature is tested with different approaches (Higuchi, 1988); the Higuchi method provides more consistent and reliable fractal dimension value for the study of fractal behavior of ULF signal (Hattori et al., 2004a; Gotoh et al., 2003; Smirnova et al., 2004). Further, multifractal techniques can better represent the different sources of the signals associated with seismicity (Turcotte, 1989). In this study, we will use nighttime Z-component geomagnetic signal as it is more sensitive to changes in local EM emissions, which are likely to be generated by microfracturing and associated lithospheric deformation. We propose to compute the fractal and multifractal dimensions of the data to extract signatures of more intense perturbations of the signal represented by higher fractal dimension values. The anomalous EM emissions can be correlated with earthquake events in search of pre-earthquake signatures. The earthquake catalog (Table T1) of the study region is adopted from the International Seismological Centre (ISC) with  $M \geq 4.5$  and epicenter within 250 km radius of recording station. 63 earthquakes are recorded from 31 March 2019 to 24 April 2020.





181

**Figure 1.** Bathymetry map of Andaman-Nicobar subduction zone including Sumatran Fault System; i.e. 182  
 Seulimeum Strand, West Andaman Fault and Andaman Trench (modified after Cochran 2010; E. Anusha 183  
 et al., 2020). The circles are representing the earthquake's location and magnitude (size of circle) 184  
 correspond to each fault system. 185

**2. Methodological Approach** 186

It is proposed to apply both fractal and multifractal approaches to the Z component time series, to 187  
 distinguish between the different source characteristics and examine their relationship to earthquake 188

parameters. The Z-component of 1 Hz geomagnetic signal analyzed because it is more prone to sense or 189  
 affected by the local EM field from lithospheric deformation in which vertical components are dominated. 190

(i) Fractal behavior of Z-component for one-day data using Higuchi is tested and examined. 191  
 Gotoh et al. (2003) tested different methods for estimation of fractal dimension of geomagnetic 192  
 signal and suggested that the fractal dimension value using Higuchi method, provided in equation 193  
 as below, is more reliable and consistent than others. In Higuchi method, a time series  $x(n)$  194  
 decomposed in to time series of different length  $x_k^m$ , defined as: 195

$$x_k^m: x(m), x(m + k), x(m + 2k), \dots \dots x\left(m + \left(\frac{N-k}{k}\right) \cdot k\right), \quad 196$$

where,  $n$  is  $1, 2, 3 \dots N$ ,  $m$  is  $1, 2, 3 \dots k$ , and  $k$  is  $1, \dots, k_{max}$ . If the average length of decomposed 197  
 time series  $L_m(k)$  computed at interval of time from  $k = 1$  to  $k_{max}$  are related to each other as: 198

$$L(k) \propto k^{-f_D}, \quad (1) \quad 199$$

then  $f_D$  is equal to the slope of fitted line over  $\log(L(k))$  versus  $\log(1/k)$  and is considered as fractal 200  
 dimension of time series data  $x(n)$ . 201

The regression line over  $\log(L(k))$  versus  $\log(1/k)$  obtained from Higuchi method (indicating power law 202  
 behaviour) of one-day nighttime (22:00-02:00 LT) Z-component of geomagnetic signal of 3 April 2019, is 203  
 shown in Figure 2. 204

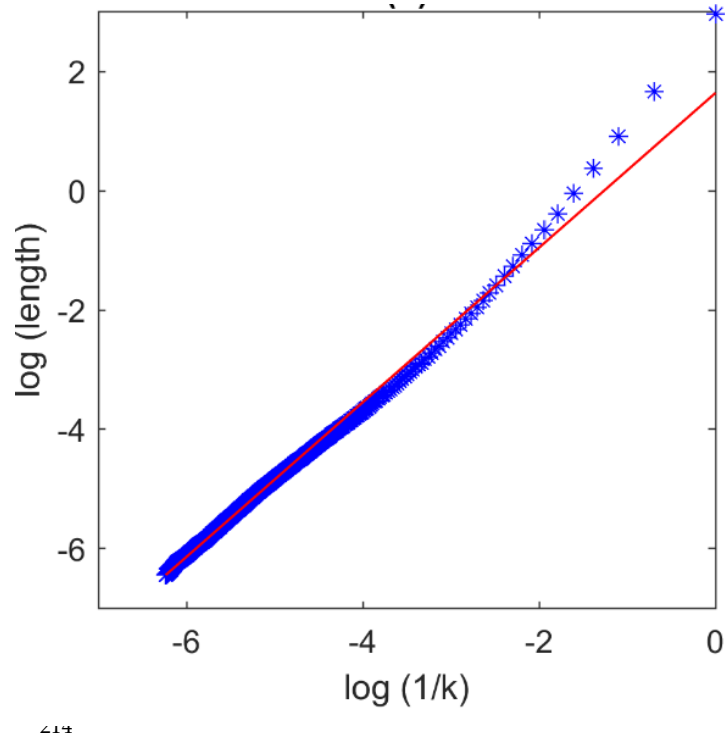


**Figure 2.** The linear fitting over log of average length and log of size of time interval (scale) showing the power law nature of geomagnetic signal.

(ii) For multifractal analyses, the Haar wavelet function is used for discrete wavelet transform because it decomposes the signal into high and low wavelet coefficients. The discrete wavelet transform decomposes the signal up to maximum level defined by  $\log_2(\text{length of } X(t))/(\text{length } (\psi_0) + 1)$ . The wavelet function  $\psi_0$  used to compute the wavelet coefficients of times series  $X(t)$  using discrete wavelet transform (DWT) ) with different level of decomposition at dyadic scale ( $2^{-j}$ ) defined as:

$$w_x(j, k) = \int X(t) 2^{-j} \psi_0(2^{-j}t - k) dt, \quad (2)$$

where,  $w_x(j, k)$  is wavelet coefficients at scale  $j$  and time  $k$ .

Further, the wavelet leader values at each level decomposition are defined from  $w_x(j, k)$ .

The wavelet coefficients in dyadic interval  $\lambda(j, k)$  at scale  $2^j$  is union of two interval at scale  $2^{j-1}$ , and 228  
 $3\lambda(j, k)$  is union of three i.e.  $\lambda_{j,k-1} \cup \lambda_{j,k} \cup \lambda_{j,k+1}$ . Thus, the largest value of coefficients occurred at scale 229  
 $2^j$  from the union of dyadic scale are referred as wavelet leaders i.e. (Lashermes et al., 2005) 230

$$L_X(j, k) \equiv L_\lambda = \sup_{\lambda' \subset 3\lambda} |w_x(d\lambda')|. \quad (3) \quad 231$$

Where,  $L_X(j, k)$  is wavelet leader at scale  $j$  and time  $k$ . 232

Since, the time series  $X(t)$  hold the condition of regularity, the wavelet leaders follow power law relation 233  
and the associated scaling exponent of  $X(t)$  at  $t_0$  is  $h(t_0)$ . The wavelet leaders selected from maximum 234  
values of wavelet coefficients at each scale provides the supreme value of scaling exponent i.e. Holder 235  
exponent. Thus, the Holder exponent  $h$  and wavelet leaders at scale  $j$  and time  $k$  at limit of fine scales  $2^j \rightarrow$  236  
 $0$  are related as (Wendt et al., 2008) i.e. 237

$$L_X(j, k) \leq C 2^{jh}. \quad (4) \quad 238$$

For the purpose of generalization of Holder exponent values, the structure function of wavelet leader is 240  
estimated at each scale ( $2^j$ ) with moment order  $q$ . The time averages of (the  $q$ th powers of) the  $L_X(j, k)$  are 241  
referred to as the structure functions (with  $n_j$ ) at scale ( $2^j$ ), which are defined as 242

$$S^L(q, j) = \frac{1}{n_j} \sum_{k=1}^{n_j} |L_X(j, k)|^q. \quad (5) \quad 243$$

Where  $n_j$  is the number of wavelet leaders at scale  $j$ . 244

Since, the time series function and wavelet leaders hold regularity condition, then the structure functions 245  
also follow power law behaviour for  $2^j \rightarrow 0$  and can be defined as (Wendt et al., 2007), 246

$$S^L(q, j) = C_q 2^{j\zeta(q)}. \quad (6) \quad 247$$

248

From above relation, the Scaling exponent  $\zeta(q)$  are computed from the structure function using regression 249

lines between  $\log 2^j$  versus  $S^L(q, j)$ , which alternatively can be defined as 250

$$\zeta_L(q) = \sum_{j=1}^2 w_j \log_2 S^L(q, j), \quad (7) \quad 251$$

where  $w_j$  is weight factor. 252

Theoretically, the function for multifractal spectrum of Scaling exponent  $\zeta_L(q)$  is based on Legendre 253

transforms, defined as 254

$$f(h) \leq \min_{q \neq 0} (1 + qh - \zeta_L(q)), \quad (8) \quad 256$$

In the present study, the equations from Wendt et al. (2007) are preferred for the computation of multifractal 257

spectrum from  $L_X(j, k)$  i.e. 258

$$f(q) = \sum_{j=1}^2 w_j U^L(j, q). \quad (9) \quad 260$$

$$h(q) = \sum_{j=1}^2 w_j V^L(j, q), \quad (10) \quad 261$$

where, 262

$$U^L(j, q) = \sum_{k=1}^{n_j} R_{X(t)}^q(j, k) \log_2 R_{X(t)}^q(j, k). \quad (11) \quad 263$$

and 264

$$V^L(j, q) = \sum_{k=1}^{n_j} R_{X(t)}^q(j, k) \log_2 L_X(j, k), \quad (12) \quad 265$$

$$R_{X(t)}^q(j, k) = \frac{L_X(j, k)^q}{\sum L_X(j, k)^q}. \quad (13) \quad 266$$

267

Larger width of multifractal spectrum indicates larger multifractality or intermittency, and vice-versa. 268

The width of multifractal spectrum  $h_w$  (from  $-q$  to  $+q$ ) indicates the overall degree of multifractality 269

of signal. The spectrum width  $h_{wp}$  ( $q > 0$ ) and  $h_{wn}$  ( $q < 0$ ) indicates the weaker and stronger 270

singularity of multifractal signal. The  $h_{max}-h_{min}$  curve defines the average fluctuations embedded in 271

the signal while  $h(0)$  represents the zero-order exponent or monofractal dimension (Hayakawa et al., 272

1999). Similarly,  $f_{max}$  define the exponent which occurred maximum number of times. Application 273

of multifractal using Haar wavelet on 30 min nighttime (22:00-02:00 LT) data of Z-component of 274

geomagnetic signal of 3 April 2019, is shown in Figure 3. 275

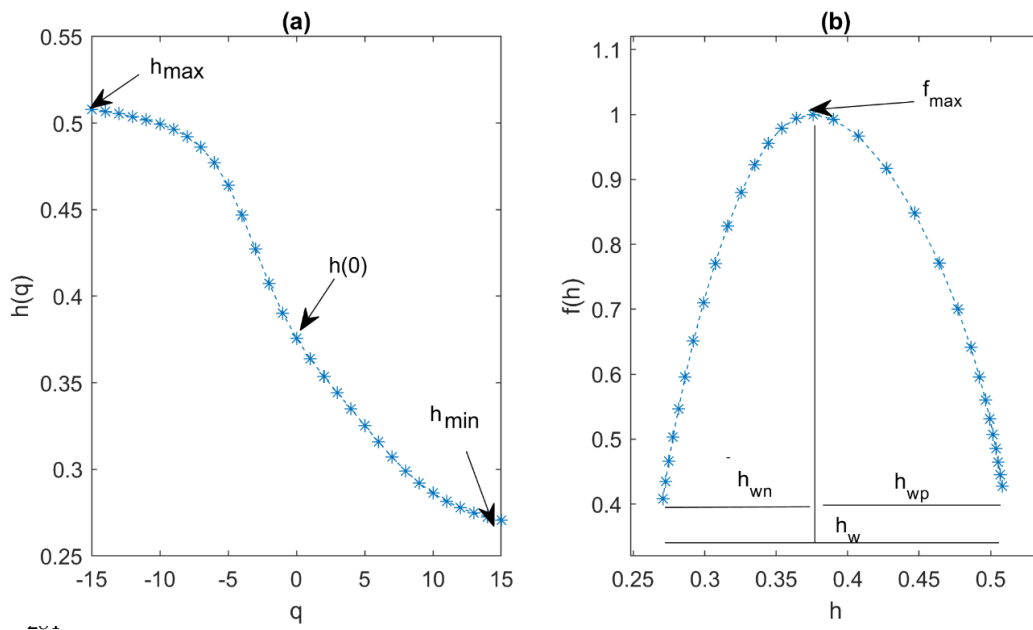


**Figure 3.** The multifractal analysis for 1800 samples of 3<sup>rd</sup> April 2019, where (a) The variation of holder 285

exponent ( $h$ ) with moment order  $q$  in range of  $-15$  to  $+15$  showing as  $h_{min}$ ,  $h_{max}$ , and  $h(0)$ . (b) 286

Multifractal spectrum showing the width of spectrum  $h_w$ ,  $h_{wp}$  and  $h_{wn}$ . 287

- (i) The high correlated values measured from fractal, is reason to select the Higuchi method, while for 289
- multifractal, wavelet leader is selected due to contact support for wide range of  $q$  ( $-q$  to  $+q$ ) and 290

stability for scaling function for negative  $q$  values compared to other techniques. From fractal, the power law behaviour, and from multifractal, the finite width of multifractal spectrum and variation in holder exponent indicates the fractal and multifractal nature of signal, respectively.

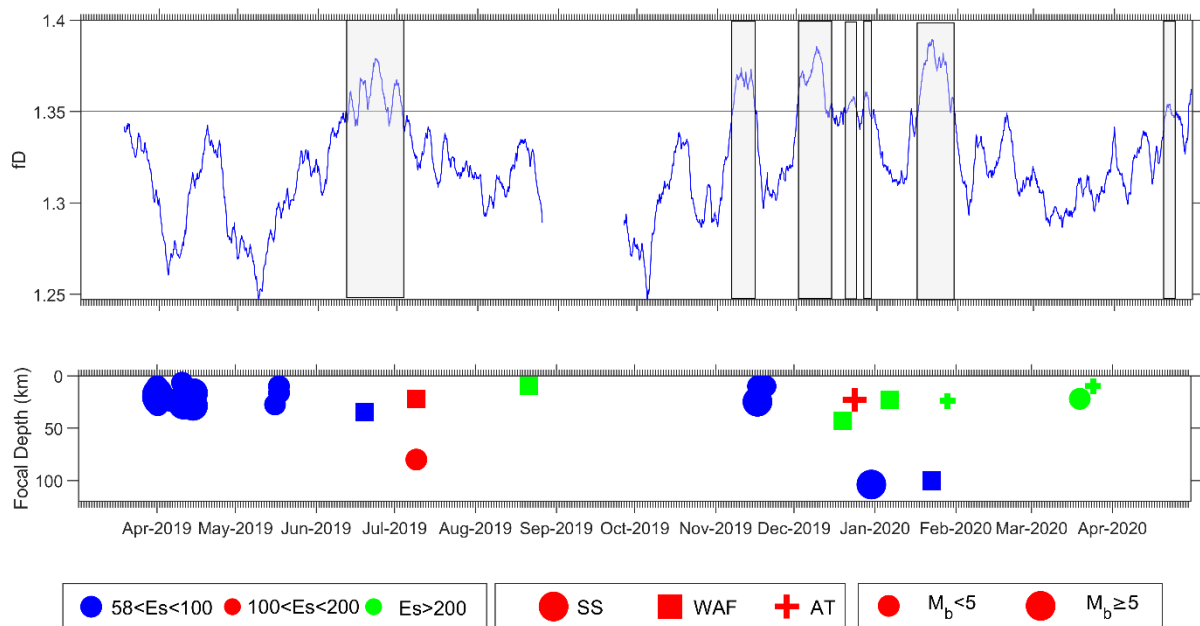
(ii) The fractal dimension  $f_D$  of the total duration of Z-component data is calculated for consecutive time windows of 30 min to trace the variations of the fractal dimension, producing eight values for each day. The choice of a 30 min time window (consisting of 1800 data points) is based on the balance between the stability of fluctuations in fractal dimension and minimizing loss of information after trials with 15 min and 1 hr. time windows.

(iii) Similarly, the spectrum width parameter ( $h_w$ ,  $h_{wp}$ , and  $h_{wn}$ ) and holder exponent parameter  $h_{max}$ ,  $h_{min}$  and,  $h(0)$  estimated for the total length of Z component from window of 30 minute to identify the degree of singularity or complexity (global, weaker, and stronger) as well as degree of fluctuations with respect to amplitude (from smaller to larger). The shorter fluctuations in fractal dimensions are smoothed by applying a 15-day moving mean.

(iv) The increments in fractal dimension and multifractal parameter (spectrum width and holder exponent) value greater than the threshold value ( $\mu + \sigma$ ) are considered as a significant increment as evidence of existence of EM signatures from lithospheric deformation.

### 3. Results

#### 3.1 Monofractal analysis



318

**Figure 4.** (a) Temporal variation of fractal dimension estimated from Higuchi method (15 days moving mean) of Z-component of geomagnetic signal. (b) The time line earthquake occurrences in same duration of geomagnetic signal.

The temporal variations in  $f_D$  of vertical component of geomagnetic signal are shown in Figure 4a;  $f_D$  greater than the threshold value 1.35 (defined by  $\mu + \sigma$ ) are indicated by grey color rectangles. The increasing fractal dimension values are directly proportional to increasing degree of complexity of signal. A synthetic test (supplementary document) of fractal dimension on fraction Brownian motion signals (fBm) with Hurst exponent 0.2, 0.4, and 0.5 i.e. monofractal signal with increasing degree of complexity (Figure S1) shows higher fractal dimension values (from Higuchi method, Figure S2) for lesser Hurst exponent signal. Moreover, combination of all three signal i.e. multifractal signal shows smaller fractal dimension values indicates that multifractal signal can't be characterized in detail using monofractal dimension. Thus, the observed enhancements in  $f_D$  of geomagnetic signal are considered as increasing



complexity from EM signatures caused by impending earthquakes. These enhanced values possibly 331  
represent the additional complexity in the signal caused by pre-earthquake microfracturing. The temporal 332  
location of enhanced fractal dimension values and their correlations with forthcoming earthquakes are 333  
summarized in Table T2. For the earthquake swarm of 1-18 Apr, 2019, and the three earthquakes of 16 334  
& 17<sup>th</sup> May, 2019, no preceding or coinciding enhancements are recorded. Two phases of enhancements 335  
during 12-13 and 16-19 Jun, 2019 occur prior to earthquake of 19<sup>th</sup> Jun, 2019 (M=4.6 of focal depth of 336  
35 km, along the WAF with epicentral distance of 60 km). The enhancements during 20-26 Jun, and 29 337  
Jun-2 Jul 2019 occur before the dual earthquakes of 9-Jul, 2019 (M=4.5-fd 80 km-epicenter distance 185 338  
km along SS fault; M=4.5-fd 22 km epicenter distance 156 km along WAF). No enhancements beyond 339  
threshold value are recorded prior to the very shallow 10 km depth earthquake of 21 Aug (M=4.8) with 340  
epicenter 219 km away along the WAF. During Sept and Oct, 2019 neither earthquakes nor enhanced 341  
fractal dimensions are observed. Three earthquakes occurred in November, two on 17<sup>th</sup> and one on the 342  
20<sup>th</sup>, all on the SS fault. They were of M 5.1, 4.5, 4.7 respectively at shallow focal depths and 343  
corresponding epicenters at 60, 91, 78 km from recording site. These events are preceded by a long 344  
duration enhancement in fractal dimension from 6-15 Nov. In December, three earthquakes occurred on 345  
19<sup>th</sup>, 24<sup>th</sup> and 30<sup>th</sup> of magnitudes 4.5, 5, 5 respectively on the WAF, AT and SS faults respectively. The 346  
earthquakes of 19<sup>th</sup> Dec of focal depth 43 km and despite large epicentral distance of 212 km from 347  
recording site, was preceded by a large amplitude and long duration enhancement of fractal dimension 348  
1-14 Dec; for the next two earthquakes of focal depths 23 and 104 km and corresponding epicentral 349  
distances of 173 and 67 km minor enhancements were observed during 18-23 Dec and 26-28 Dec. For 350  
the three earthquakes of Jan 2020, the M 4.5 shallow earthquake of 6<sup>th</sup> Jan with epicentral distance >200 351  
km, no enhancements are observed. The earthquakes of 22<sup>nd</sup> and 28<sup>th</sup> Jan occurred. No earthquakes were 352

recorded in Feb 2020 and no anomalous enhancements are observed. During March 19<sup>th</sup> and 24<sup>th</sup> there were two shallow M=4.5 earthquakes with epicentral distances more than 200 km along the SS and AT respectively. During 20-22 Apr, a small enhancement is observed, the succeeding earthquake is not included in present catalogue.

### 3.2 Multifractal analysis

The holder exponent curve and multifractal spectrum width are calculated for the same data of 3<sup>rd</sup> April, 2019 for the 30 min interval 22:00 – 22:30 LT, with 1800 data points. The large variation in Hurst exponent against moment order  $q$  (Figure 4a) and wide width of multifractal spectrum of geomagnetic time series (Figure 4b) indicate the multifractal nature of geomagnetic signal. The multifractal behavior of a signal is generally characterized by the width of multifractal spectrum ( $h_w$ ) as well as spectrum width  $h_{wn}$  correspond to  $-q$  to 0 and  $h_{wp}$  correspond to  $+q$  to 0 also assist in characterizing the specific nature of the geomagnetic signal (Figure 4). Apart from spectrum width parameter, holder exponent parameters, such as  $h_{min}$ ,  $h_{max}$ ,  $h(0)$ , and  $f_{max}$  are also useful to characterize the nature of pre-earthquake geomagnetic signal (Figure 4).

#### 3.2.1 Multifractal spectrum width

The width of multifractal spectrum deciphers the nature of complexity of analyzed signal; higher spectrum width indicates larger degree of heterogeneity. A synthetic test of multifractal spectrum on fraction Brownian motion signals (fBm) with Hurst exponents 0.2, 0.4, and 0.5 show increasing width of multifractal spectrum respectively (Figure S3). Moreover, the multifractal spectrum width of combined signal show highest values, indicating increasing nature of complexity, which was not accurately determined by the monofractal dimension. The width of multifractal spectrum ( $h_w$ ,  $h_{wp}$  and  $h_{wn}$ ) of a sliding window of 1800 data points (half an hour) without overlapping is computed for whole time series

of vertical component of Z-component (Figure 5). The 15-day moving mean of variation in spectrum width of multifractal spectrum shows significant variations in the range of 0.09 to 0.26. Enhancements greater than threshold value ( $\mu + \sigma$ ) are considered as an anomaly in fractal dimension; . Enhancement in at least one of the components  $h_w$ ,  $h_{wp}$  and  $h_{wn}$  is considered as significant perturbation of the geomagnetic signal (Figure 5). The enhancements in  $h_w$ ,  $h_{wp}$  and  $h_{wn}$  components with corresponding earthquakes is summarized in Table T3. For the earthquake swarm of 31 Mar-18 Apr, 2019 (moderate magnitude 4.5-5.3, shallow focal depth 15-30km, and epicentral distance 50-100 km), a preceding enhancement (in  $h_w$ ,  $h_{wp}$ , and  $h_{wn}$ ) component occurred during 17-22 Mar, 2019. The significant enhancement during 14 May (in  $h_w$  component), 14-15 and 17-20 May, 2019 (in  $h_{wp}$  component) and 29Apr-5 May, 2019 (in  $h_{wn}$  component) are partly common to each other and occurred prior, co and post of earthquake 16<sup>th</sup> and 17<sup>th</sup> May, 2019 (moderate magnitude (4.5-4.8), focal depth (10-27.4), and epicentral distance (58-71)). The two sets of enhancement during 22-25 May, 2019 and 4-22 Jun, 2019 (in  $h_w$  and  $h_{wp}$ ) and one persistence enhancement during 8-22 Jun, 2019 occurred prior to earthquake 19 Jun, 2019 (M 4.6, focal depth 60 km, and epicentral distance 60 km). the enhancement in common duration 30-9<sup>th</sup> Jul, 2019 (different duration of persistence) and no enhancement in  $h_{wn}$  component occurred prior to two earthquakes 9<sup>th</sup> Jul, 2019 at two different locations with moderate magnitude (4.5), moderate and shallow focal depth (80 and 22 km) and large epicentral distance (185 and 156 km). The common enhancement during 17-19<sup>th</sup> Jul, 2019 in  $h_w$  and  $h_{wn}$  component (not same duration of persistence) occurred prior to earthquake on 21<sup>st</sup> Aug, 2019 (M 4.8, focal depth 10 km, and large epicentral distance 219 km). the common enhancements during 9-15 Oct, 2019, 7-10<sup>th</sup> Nov, 2019, in  $h_w$  and  $h_{wp}$  component, 11-12<sup>th</sup> Nov in  $h_w$ , and 2-3, 12-14<sup>th</sup> Nov, 2019 in  $h_{wp}$  component occurred prior to earthquake 17<sup>th</sup> and 20<sup>th</sup> Nov, 2019 with moderate magnitude (4.7-5.1), focal depth (10-25 km), and

epicentral distance (60-91 km). Further, the four-earthquake occurred during December, 2019 and 1<sup>st</sup> week of Jan, 2020 is not (moderate magnitude, moderate focal depth, and moderate to large epicentral distances) preceded by any significant enhancement in components of multifractal width parameter. The common enhancements during 16-20 Jan, 2020 in  $h_w$  and  $h_{wp}$  component occurred prior to earthquake 22<sup>nd</sup> (M 4.6, focal depth 100km, and epicentral distance 77) and 28<sup>th</sup> Jan, 2020 (M 4.9, focal depth 24km, and epicentral distance 204 km). Further, the two-earthquake event of May-2020 (moderate magnitude, shallow focal depth, and large epicentral distance) is not preceded by any enhancement in components of multifractal width parameter.

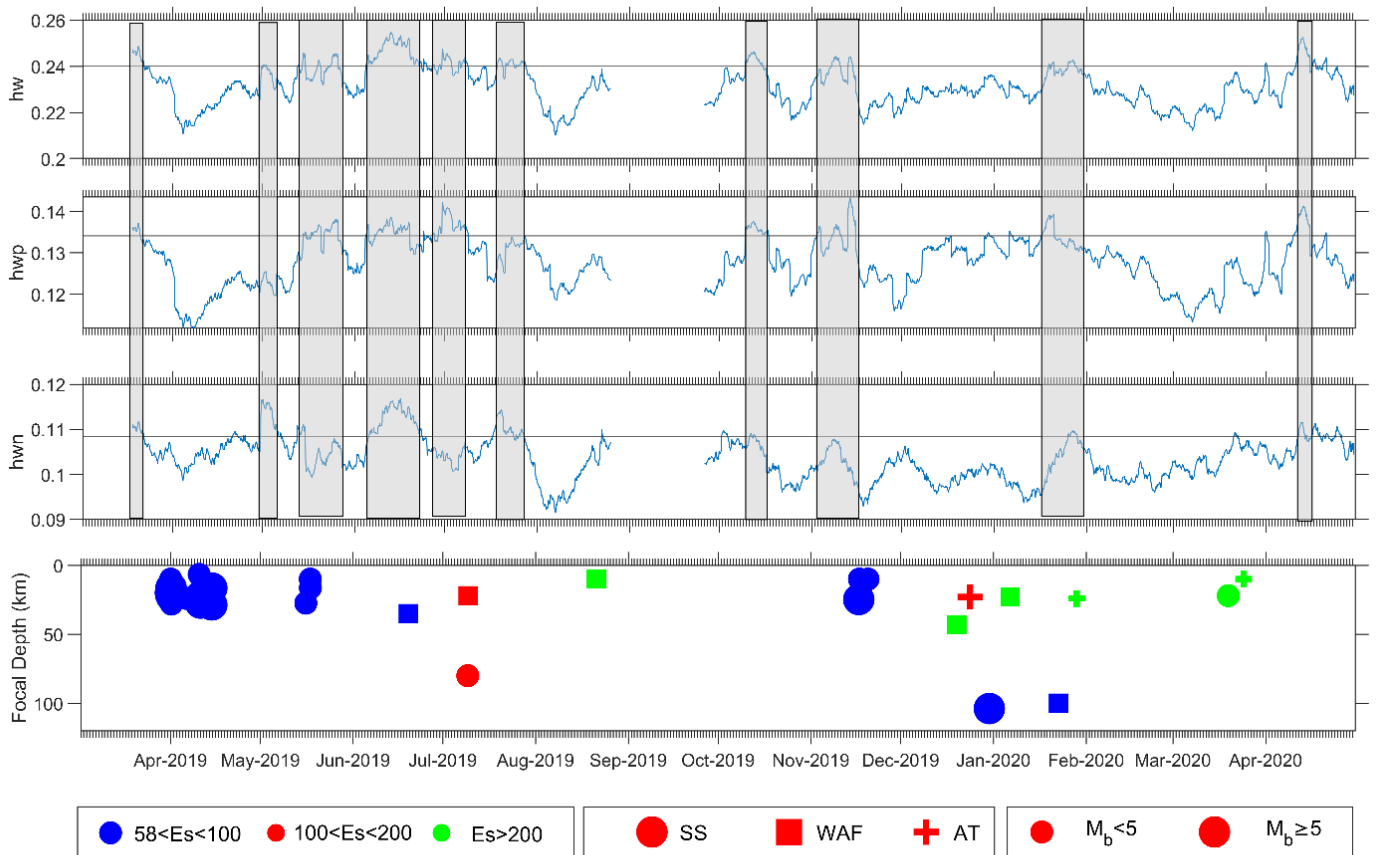
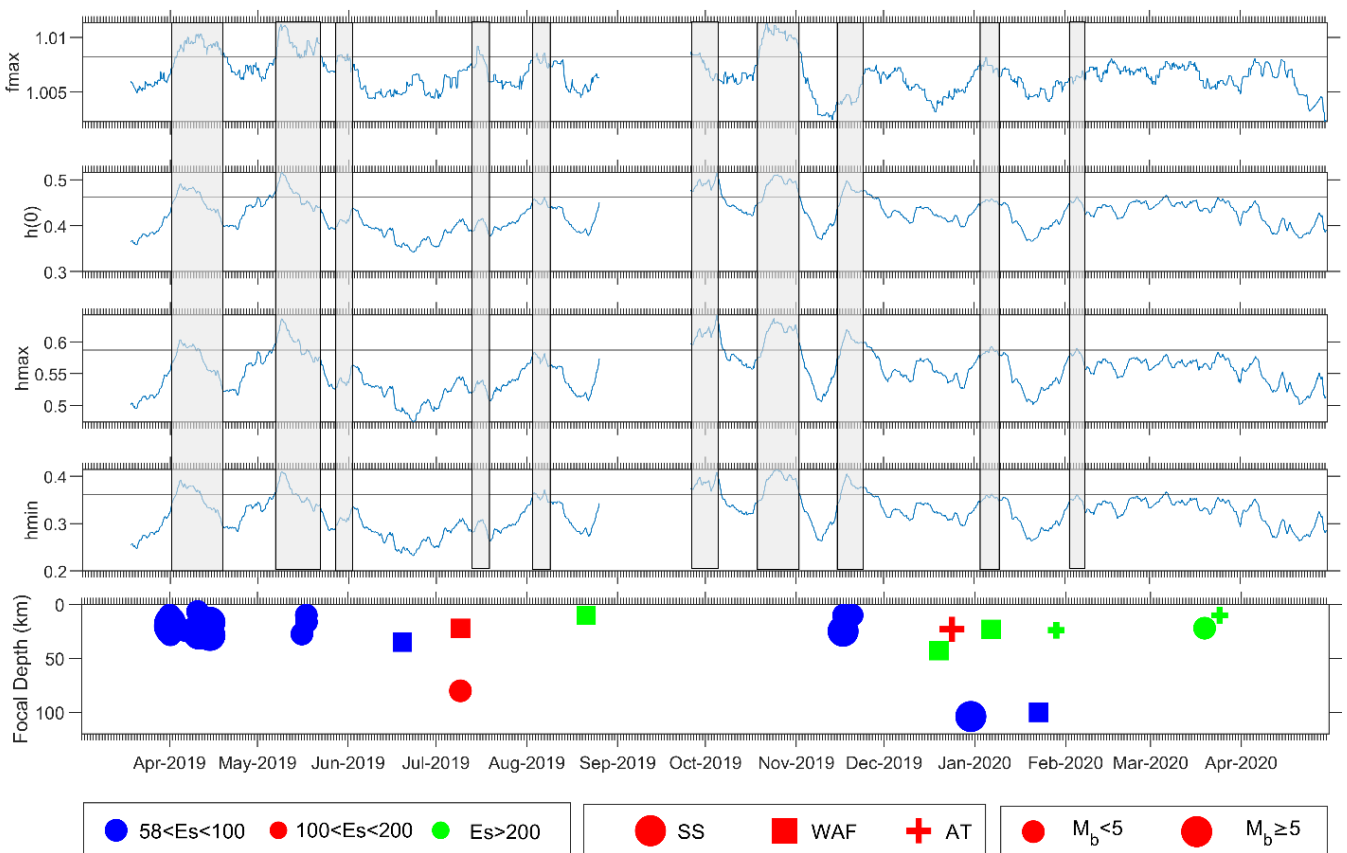


**Figure 5.** Temporal variation in spectrum width  $h_w$ ,  $h_{wp}$  and  $h_{wn}$  from top panel and anomalous behavior are highlighted by grey color. The bottom panel showing the occurrences of earthquake with magnitude (size of circle) and corresponding faults (different color). Top four panel showing the detail view of Jun 2019 month.

### 3.2.2 Holder Exponent

The holder exponent parameters ( $h_{max}$ ,  $h_{min}$ ,  $h(0)$ , and  $f_{max}$ ), used for defining the multifractal spectrum curve also show significant variations in the amplitude; again enhancements greater than threshold value (1.0082, 0.4626, 0.5873, 0.3612) are treated as significant (Figure 6). The enhancements in  $h_{max}$ ,  $h_{min}$ ,  $h(0)$ , and  $f_{max}$  components with corresponding earthquakes are summarized in Table



T4.

**Figure 6.** Temporal variation in holder exponent parameters i.e.  $f_{max}$ ,  $h_{fmax}$ ,  $h_{max}$  and  $h_{min}$  from top panel and anomalous behaviour are highlighted by grey colour. The bottom panel showing the occurrences of earthquake with magnitude (size of circle) and corresponding faults with different color.

The common enhancements during 2-18 April, 2019 in all components of holder exponent coincide with the swarm of earthquake 31<sup>st</sup> 18<sup>th</sup> April, 2019 with moderate magnitude, moderate focal depth, and moderate to large epicentral distance. The next common enhancements are noted during 6-14 May, 2019 in all components of holder exponent prior to the three earthquakes (moderate magnitude, focal depth and epicentral distance), one 16<sup>th</sup> May, 2019, and two 17<sup>th</sup> May, 2019. For the same earthquakes two small co and post seismic enhancements are noted in  $f_{max}$  component during 17-19 May, 2019. The small enhancement in only  $f_{max}$  during 20-21 May, 2019 is preceded by the earthquake 19<sup>th</sup> Jun, 2019 with moderate magnitude, focal depth, and epicentral distances. Further, the two-earthquake event of 9<sup>th</sup> July with moderate magnitude, epicentral distance, large epicentral distance and different location is not preceded by enhancements in any component of holder exponent. Two small enhancements during 15-16 Jul, and 6 Aug, 2019 in  $f_{max}$  component and two small enhancements in  $h_{min}$  during 6 Aug, 2019 occurred prior to the earthquake 21 Aug, 2019. The two enhancements common in all components but different durations, one small during 26 Sep-5Oct, 2019 and persistence during 16 Oct-24 Nov, 2019 occurred prior as well as coincident and post three earthquakes. Two of them were at similar location 17<sup>th</sup> Nov, 2019 and one at a different location 20<sup>th</sup> Nov, 2019 with moderate magnitude, shallow to very shallow earthquake, and moderate epicentral distance. Further, the three-earthquake occurred in December, 2019, the first two with moderate magnitude and focal depth and large epicentral distance and third with moderate magnitude, large focal depth, and moderate epicentral distance are not preceded

by enhancement in any component of holder exponent. The next small enhancement in  $h_{max}$  component 437  
 only during 3-8 Jan, 20020 is coincident with earthquake of 06<sup>th</sup> Jan, 2020 (mod. Magnitude, mod. Focal 438  
 depth, and large epicentral distance) and preceded by two earthquakes on 22 and 28<sup>th</sup> Jan, 2020 (with 439  
 moderate magnitude, moderate and large focal depth; large and moderate epicentral distance). 440

For the earthquake swarm of 31 March, 2019 and early April, the spectrum width shows a small 441  
 enhancement during 17-20<sup>th</sup> March, that is 12 days prior to the earthquake cluster, which have 442  
 magnitudes between 4.5 to 5.3 and occur in a small region along the SS fault. There is no enhancement 443  
 of the Holder exponent. For the intermittent earthquakes in mid-April, there is no signal in the spectrum 444  
 width but the Holder exponent shows a consistent enhance during 3-10 April, a week before the main 445  
 cluster. In early May, upto 5<sup>th</sup>,  $h_{wn}$  shows an enhancement; the pattern is mimicked in the Holder 446  
 exponent without crossing the threshold value. Small anomalous enhancements 12-14<sup>th</sup> May on the  $h_{wn}$ , 447  
 $h_{wp}$  and  $h_w$  of spectrum width, just prior to the moderate earthquakes on 16<sup>th</sup> and 17<sup>th</sup> May. The holder 448  
 exponent exhibits a longer, more consistent enhancement during 7-14<sup>th</sup> May,  $f_{max}$  shows a co-seismic 449  
 anomaly on 17-19 May, followed by anomalies on 20-21 May. Post seismic perturbations are also noted 450  
 in the spectrum width. For the M4.6 earthquakes of 19<sup>th</sup> June, long duration anomalies are seen in 451  
 spectrum width but not in Holder exponent. For the dual earthquakes on 9<sup>th</sup> July, pre and post seismic 452  
 anomalies are seen in spectrum width; only one anomaly is seen in Holder exponent during 14-16 June. 453

There is no significant multifractal anomaly for the 21 Aug, very shallow earthquake. In October 2019, 454  
 significant repeated anomalies are observed in Holder exponent right till Nov, 2019. In the second half 455  
 of Jan and much of February, there are several individual earthquakes; no significant enhancement is 456  
 observed for any of them. A short enhancement can be noted in 11-14 April, which would be indicative 457  
 of a future event. 458

### 3.3 Combined result of monofractal and multifractal analysis

Figures 4, 5, and 6, show that all the components from monofractal and multifractal, have different response for each earthquake, indicating different characteristics of signal, which can be used as indicator of pre-earthquake processes in the focal zone of earthquake. In this regard, we have characterized the enhancements of components in three types of patterns: (i) present in only monofractal component, (ii) present in only multifractal components, and (iii) present in monofractal as well as in multifractal component. The significant enhancement from both parameter (monofractal and multifractal) with corresponding earthquake from figure 4, 5, and 6 is summarized in Figure 7.



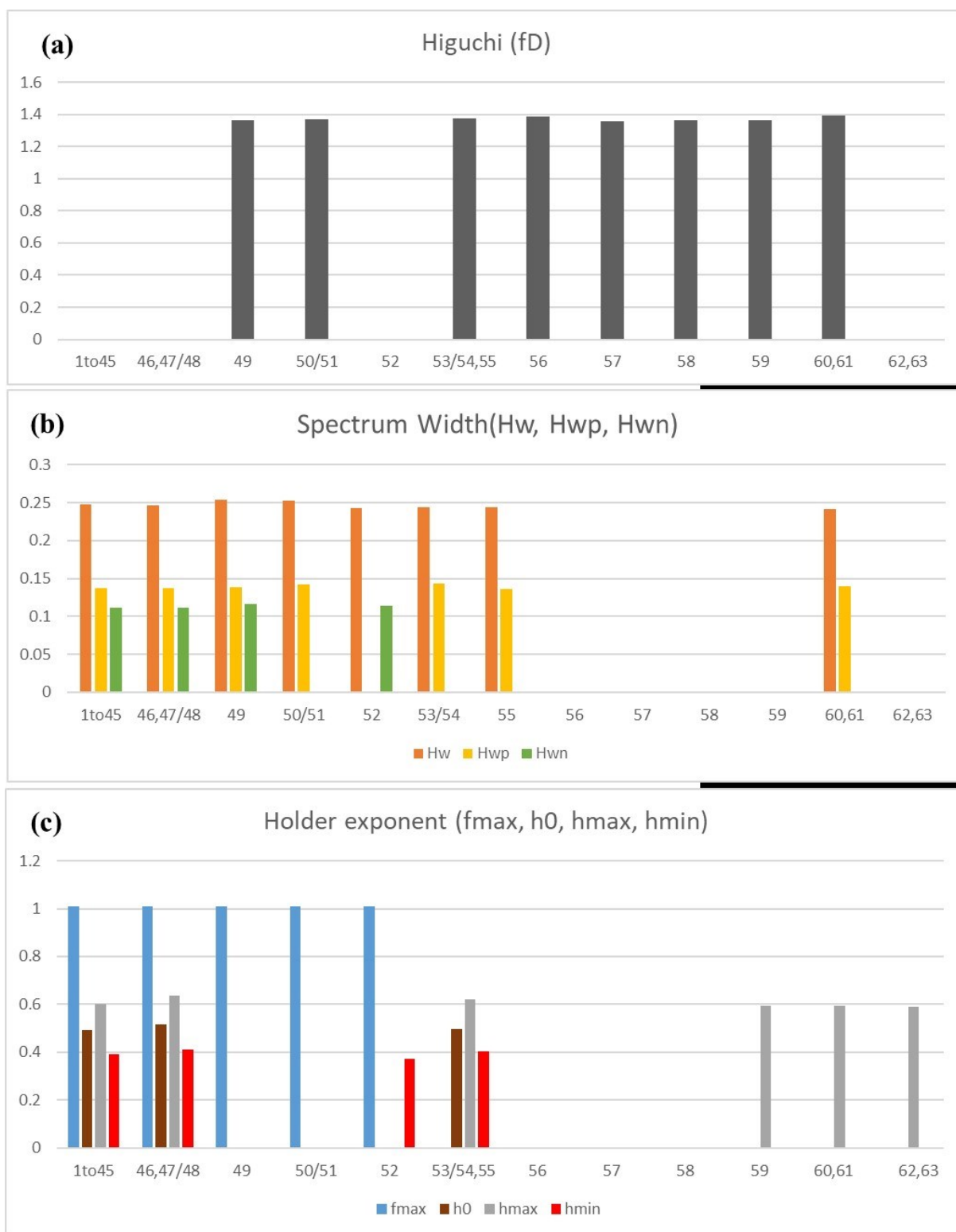
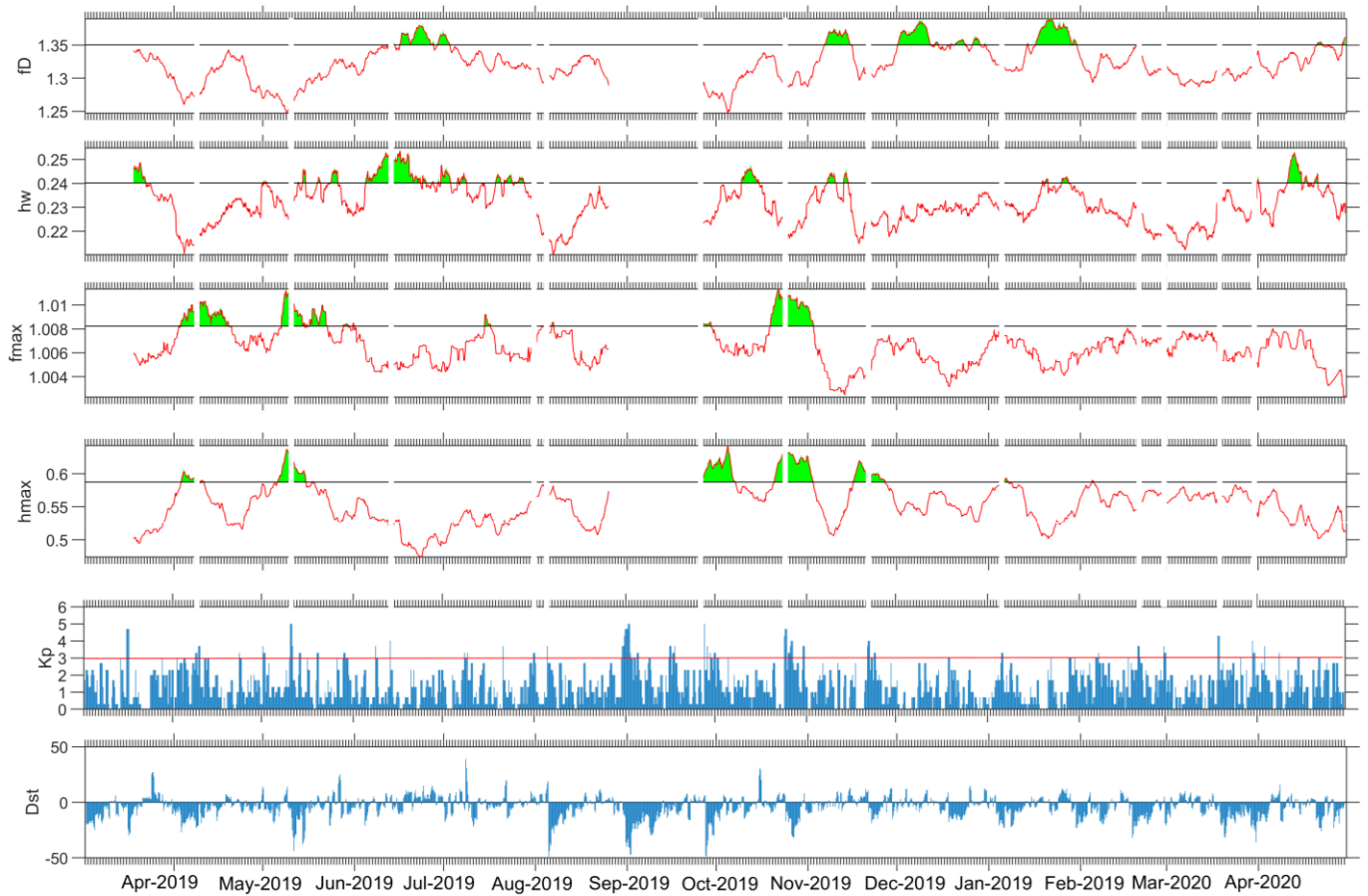


**Figure 7.** The components of significant enhancement with corresponding earthquakes from (a) Higuchi 499  
fractal dimension, (b) Spectrum width, and (c) Holder exponent. 500

From Figure 7 it is evident that the Higuchi fractal dimension from monofractal analysis exhibits significant enhancements corresponding to earthquake 56, 57, and 58, while there are no enhancements in multifractal component correspond to same earthquake. Furthermore, there are significant enhancements in multifractal components correspond to the earthquake 1-45 (swarm of earthquake), 46, 47/48, 52, 62, and 63, while there are no enhancements in monofractal component (or Higuchi fractal dimension). It is also noted that the earthquake 1-45, 46, 47/48 exhibit to all component of spectrum width ( $h_{wn}$ ,  $h_{wp}$  and  $h_w$ ) and holder exponent  $f_{max}$ ,  $h_{max}$ ,  $h_{min}$ , and  $h(0)$ , while for earthquake 52 ( $h_w$ ,  $h_{wn}$ ,  $h_{min}$ , and  $f_{max}$ ), 62 ( $h_{max}$ ), and 63 ( $h_{max}$ ) all components of multifractal parameters are not present. Similarly, the significant enhancements correspond to earthquakes 49, 50/51, 53/54, 55, 59, 60, and 61 observed in monofractal as well as multifractal components, but not in all components of multifractal. From multifractal parameters it is also noted that,  $h_w$  component of spectrum width is present in each enhancement,  $h_{max}$  component is present with each except for the 49, 50/51, and 52 earthquakes. Similarly, enhancements in  $f_{max}$  along with spectrum width  $h_w$  is present for all the earthquakes except 53/54, 55, 60, 61. Significant enhancements for days where the Kp index is greater than 3 and Dst index smaller than -50 have been identified and removed from the study, although such short duration effects are diminished considerably after averaging of each component with 15 day moving mean (Figure 8). An additional component of diurnal ratio is also appended for correlation with monofractal and multifractal components, which is also treated with criteria of planetary index (figure 8).



521

522

**Figure 8.** Temporal variation of (a) Higuchi fractal dimension, (b) spectrum width component of multifractal width parameter, (c)  $f_{max}$  component, and (d)  $h_{max}$  component after removing the data correspond to (f)  $K_p > 3$  and (g)  $Dst < -50$ .

523

524

525

Therefore, from multifractal analysis,  $h_w$ ,  $h_{max}$ , and  $f_{max}$  components, and Higuchi fractal dimension from monofractal parameter has traced all the significant signatures corresponding to the seismogenic activity in the earthquake. The month-wise analysis from Mar-2019 to April -2020 of each component preferred for detail analysis of enhancements shown in Figure S4-S17. From the total duration of analysis, we have selected two quiet days 25<sup>th</sup> May and 3<sup>rd</sup> Aug – 2019 and shown the geomagnetic field variation on corresponding date (figure S18), in which first is showing quite disturbed signatures (also showing high multifractal values) compare to second (showing smaller multifractal values). This

526

527

528

529

530

531

532

suggests that the disturbance in geomagnetic field on the quiet day 25<sup>th</sup> May, 2019 is highly possible due to interference of EM fields.

### **Discussion:**

We examine the combined observations of signatures from monofractal or Higuchi fractal dimension ( $f_D$ ) and multifractal components ( $h_w$ ,  $h_{max}$  and  $f_{max}$ ) along with diurnal ratio to unravel a linked pattern, which can be interpreted as related to earthquake processes (Figure 9). A swarm of earthquakes (1-45 as per our catalogue) along the SS fault occurred around the first week of April 2019. The data is available from 15<sup>th</sup> March and no anomalies were identified in the Diurnal ratio; hence it was concluded that data length was insufficient (Prajapati and Arora, 2024). While no anomalies were detected in the  $f_D$ , distinct enhancements are noted in the Spectrum width 14 days prior to the beginning of the swarm. Co-seismic  $f_{max}$  over the entire duration and muted  $h_{max}$  enhancements are noted during 2-18 April and 2-10 April respectively.

For the moderate magnitude, shallow focus earthquakes 46, 47, 48, clustered close together during mid-June 2019, Diurnal ratio shows a significant enhancement 50 days before the events, whereas no anomalies are recorded in  $f_D$ . Enhancements in both  $h_{max}$  and  $f_{max}$  start 11 and 9 days before the events and continue co-seismically.

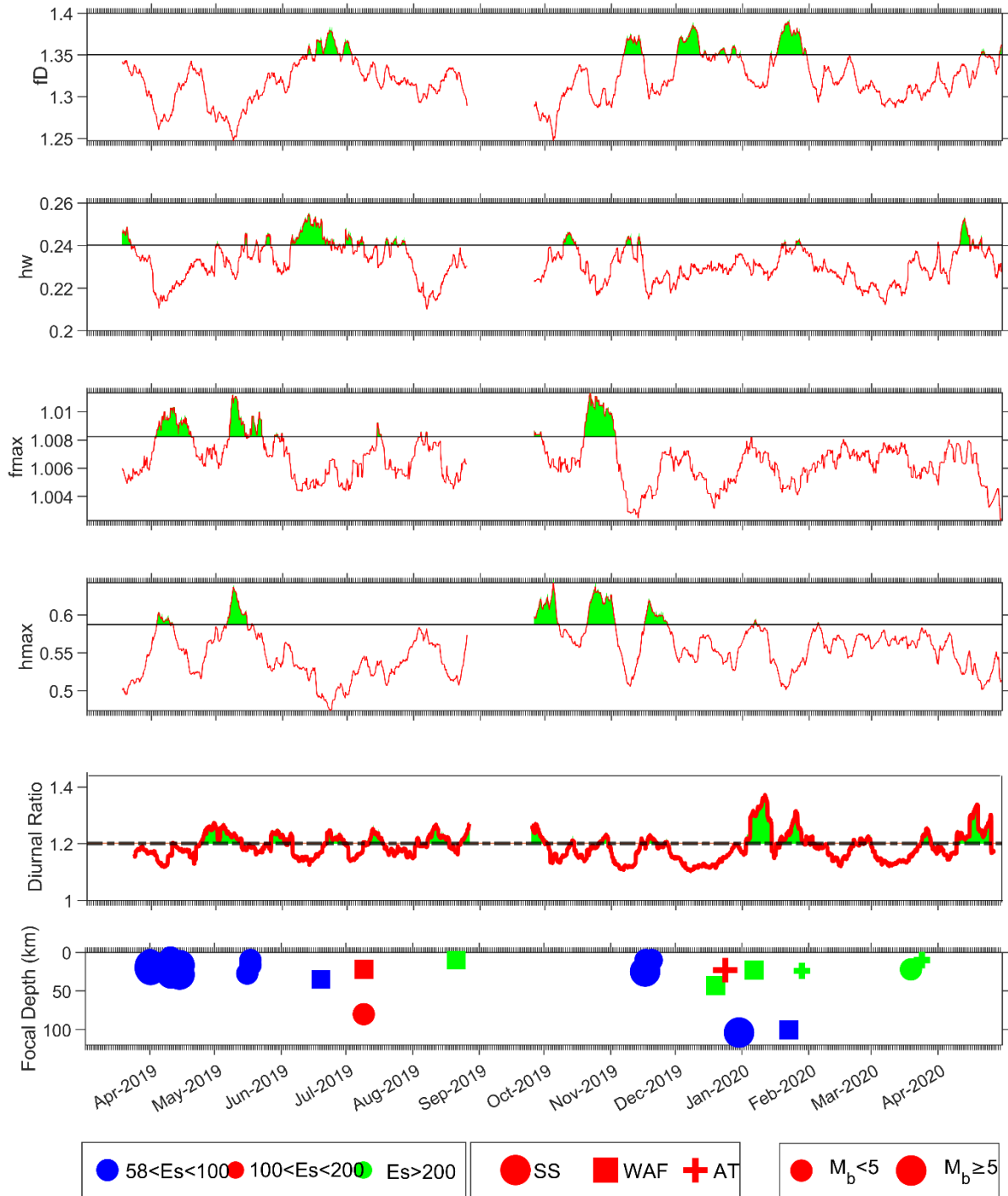


**Figure 9.** The significant enhancement in temporal variation of (a) Higuchi fractal dimension, (b) 573  
spectrum width component of multifractal width parameter, (c) fmax component showing the holder 574  
exponent presence highest number of time (d) hmax component showing the largest value of holder 575  
exponent, and (e) diurnal ratio, indicated by shaded green color, (f) the occurrences of earthquakes in 576  
same time duration with magnitude and focal depth. 577

Earthquake 49 on 19<sup>th</sup> June 2019 was of moderate magnitude, moderate focal depth and moderate epicentral distance on the WAF. It is preceded by small enhancement in Diurnal ratio 22 days before,  $f_D$  7 days prior and continues co-seismically. Spectrum width enhancement starts 15 days prior to event, which continues co-seismically, there are no signatures in  $h_{max}$  or  $f_{max}$ .

The dual earthquakes 50 and 51, occurred soon after 49, at large epicentral distances on the WAF (shallow focal depth) and on the SS (deep focal depth) in opposite directions to the recording station. Diurnal ratio shows a significant anomaly 16 days prior to the event, accompanied by slight increase in  $f_D$  19 days before. Mild perturbations are also observed in Spectrum width 9-4 days before the events.

The earthquake 52 is similar to 49, with shallower focal depth and very large epicentral distance of 219 km on the WAF. It is preceded by enhancement in Diurnal ratio is seen 14 days before, no signatures are seen in any other parameter.

The earthquakes 53, 54, 55 on 17 and 20 Nov 2019, occur along the SS fault with moderate epicentral distances and shallow focal depth; 53 has magnitude of 5. They are preceded by two phases of small enhancements in Diurnal ratio 21 and 3 days before the earthquakes, continuing to co-seismic signatures. Enhancements in  $h_{max}$  continue to co-seismic signatures. Signatures in  $h_w$  are very muted,  $f_D$  shows significant enhancement 2 days prior to the earthquakes.

Earthquakes 56-63 are individual events, from end of 2019 to first quarter of 2020, separated by several days to weeks intervals in between. Earthquake 56 has very large epicentral distance, also occurring on the WAF like earthquake 52, but with a focal depth of 43 km. This is followed by 57, which is a M=5 earthquake at very shallow focal depth, at large epicentral distance on the AT. Earthquake 58 occurred on Dec 30, 2019, an M=5 event on the SS fault with large focal depth and moderate epicentral distance. The events are preceded by a significant enhancement in  $f_D$ , but no other signatures. With only one station, it

is not possible to construct an earthquake-anomaly link for this scenario. The cluster of 53-54-55, for which signatures are noted in Diurnal ratio,  $f_D$ , and  $h_{max}$ , occurred in a closer duration period, on the same SS fault at moderate epicentral distances and are also at shallow focal depth. The earthquake 59 is of moderate magnitude, shallow focal depth but large epicentral distance on the WAF. Curiously, a co- and post seismic enhancement in diurnal ratio is the sole signature for this event. For the earthquakes 60 (large focal depth and moderate epicentral distance on the WAF) and 61 (shallow focal depth and large epicentral distance on the AT), co-seismic enhancement in diurnal ratio is accompanied by similar enhancement in  $f_D$ . Earthquakes 62 (moderate magnitude, shallow focal depth and large epicentral distance on the AT) and 63 (moderate magnitude, shallow focal depth and large epicentral distance also on the AT), no preceding signatures are observed on any of the parameters. However, a distinct post seismic increase in diurnal ratio is noted.

In April 2020, enhancements in  $h_w$  during 10-14 April and Diurnal ratio during 10-24 April are observed. Several research articles are available (Hayakawa et al., 1999; Gotoh et al., 2003; Ida et al., 2012) to study the behavior of geomagnetic signal using non-linear signal processing techniques such as monofractal and multifractal in context of EM field generated from local sources due to seismogenic activity. Hayakawa et al. (1999) have analysis on H, D, and Z component of ULF geomagnetic signal recorded at 65 km from the epicenter of Guam earthquake (M=8) occurred on 8<sup>th</sup> Oct, 1993 at focal depth of around 60 km carried using fractal (spectral method) and Hurst exponent analysis (rescaled scaled range R/S method). They inferred that decreasing value of slope ( $\beta$ ) from 2.5 to  $\sim 1$  before the earthquake, which can be considered as an indicator of SOC, where  $\beta \sim 1.1$  is critical value prior to the earthquake. However, no significant changes observed in Hurst exponent by R/S analysis. The large-scale variation and decrease in ULF spectrum slope (or increase in fractal dimension) means increase high frequency fluctuations is a proxy

measure of small-scale fractal structure cause by active microfracturing process followed by generation of 622  
seismogenic ULF emission. In our study, we have also noticed the increase in fractal dimension atleast 10 623  
days prior to the earthquake (49,50-51,53-55, and 60-61) with moderate magnitude ( $4.5 < M < 5.1$ ), shallow 624  
and moderate focal depth (35, 51,14, and 62km), as well as small, moderate, and large epicentral distance 625  
(60, 170, 76, and 140km). The increasing fractal dimension before the earthquakes are suggests the 626  
microfracturing process in Earth's crust to be the cause of generation and emission of EM field in the 627  
vicinity of recording station. 628

Gotoh et al. (2003) have analyzed the ULF geomagnetic data recorded at three stations on Izu peninsula, 629  
Japan, where a nearby strong earthquake swarm started from 26, June to August 2000 with magnitude upto 630  
6.5. An eruption of volcanic also started simultaneously in Miyakejima Island. Izu region on Philippine 631  
plate is under tensile stress and seismically very active because of subduction of Pacific plate at Nankai 632  
and Sagami Troughs (Uyeda et al., 2002). The monofractal dimension of the H component shows an 633  
increase a week before the earthquake. In present study, we have analyzed Z-component instead of H- 634  
component, because recent studies suggested that Z-component is more sensitive for EM fields generated 635  
from local sources. In our study we did not find any significant signature of enhanced fractal dimension of 636  
Z component one week prior to a swarm of 45 earthquakes from 31-Mar to 18-April, 2019, however an 637  
enhancement in spectrum width parameter ( $h_w$ ), 10 days before the swarm activity started. 638

Further, Ida et al. (2005) carried out the multifractal analysis on H component of geomagnetic signal 639  
recorded at 65 km from the epicenter of Guam earthquake occurred on 8<sup>th</sup> Oct, 1993 at focal depth of around 640  
60 km. A westward movement of the Pacific plate and its subduction under Philippine plate triggered the 641  
Guam earthquake ( $M_s$  8.0) at shallow dipping subduction zone with a strike slip fault along the trench 642  
(Harris, 1993). Ida et al. (2005) found significant changes in the multifractal parameters of Holder exponent 643



and spectrum width ( $\alpha_{min}$ ,  $\alpha_{max}$ ,  $w$ ,  $\Delta$ ,  $f_{max}$ ,  $\alpha(f_{max})$ , and  $D_q$ , for  $q < 0$ ,  $q > 0$ , and  $q = 0$ ). The 644  
observation of 9 days running mean of spectrum width  $w$  and  $\alpha_{max}$  shows clear and significant variation 645  
30 days prior to the earthquake. In our analysis of multifractal parameters from moderate subduction zone 646  
earthquakes, with focal depth in range of 10-30 km, the 15-day running mean of Spectrum width and Holder 647  
exponent show significant enhancements 12 and 20 days prior to those earthquakes, which occurred close 648  
in time as a cluster (1-45, 47-48, 50-51, 53-55). This difference in pattern may be due to the large 649  
differences in magnitude of the studied earthquakes. 650

Ida et al. (2012) analyzed the fractal dimension (estimated by Higuchi method) of ULF data recorded at 651  
Kashi station, China, approximately for four years (Mar, 2003 to Dec, 2006), in which several moderate 652  
earthquakes occurred (greater than 5.0 and close to 6) at epicentral distances of 100 to 125, including one 653  
earthquake at approximately 300 km. The region is seismically very active due to relative movement of 654  
plates along SAF fault (normal fault) is locally dominant in the area (He et al., 2015). Ida et al. (2012) 655  
applied the criterion of  $\mu \pm 2\sigma$  to define the significant variations of the fractal dimension and reported 656  
decrease in the Z component for two earthquakes (M 5.7 and M 5.4) while the other earthquakes with 657  
magnitude greater than 5 did not show any signature. The enhancement in  $f_D$  is interpreted as indication of 658  
dominance of high frequency component and decrease in  $f_D$  as dominance of low frequency component, 659  
which may correlate with the high frequency mechanism like micro-fracturing and slow processes like 660  
electrokinetic effect respectively. Potirakis et al. (2017) has analyzed geomagnetic data (H, D, and Z) at 661  
station Kakioka (KAK) at epicentral distance of 300 km from Tohoku earthquake (M 9.0) of 11 March, 662  
2011. The earthquake was caused by the rupture of a stretch of the subduction zone associated with 663  
the Japan Trench, which separates the Eurasian Plate from the subducting Pacific Plate. The data analyzed 664  
using DFA and Higuchi method, observed a significant decrease in spectral exponent (using DFA) and 665

corresponding increase in fractal dimension (using Higuchi method) 5-6 months prior to the large 666  
magnitude Tohoku earthquake. In our study, we have found significant enhancements with the criterion of 667  
 $\mu + \sigma$ , producing pre-seismic increases in  $f_D$  for multiple earthquake occurrences (50-51, 53-55) with 668  
 $4.6 < M = 5$  and either shallow focal depth or small epicentral distance, 19 and 11 days before the earthquakes. 669  
The concept of self-similarity in time series data was introduced by Mandelbrot and Van Ness (1968) and 670  
has been used to investigate patterns of seismicity to improve their predictability, as early as the 1990s, e.g. 671  
Godano and Caruso (1995), who showed that multifractal characteristics of seismic catalogues are more 672  
appropriate, indicating varying degrees of clustering of seismic events. Fractal analysis has been used to 673  
study the fractal characteristics of geomagnetic field data to reveal the complexity and irregularity of the 674  
geomagnetic field, and how it changes in response to different conditions. For example, analysis of the 675  
fractal properties of the geomagnetic field during different activity levels, showed that the geomagnetic 676  
field is more multifractal during quiet periods than during storms, and that the scaling properties of the 677  
field show long-term persistence (Babu and Unnikrishnan, 2023). Another study used the Higuchi 678  
method to calculate the fractal dimension of the geomagnetic field at a Russian magnetic station and 679  
found correlations between the fractal dimension and solar wind characteristics and the Auroral Electrojet 680  
(AE) index (Gvozdev and Parovik, 2023) and for studying geomagnetic secular variations (Sridharan 681  
and Ramasamy, 2006). Over the last 20 years many workers have examined the fractal characteristics of 682  
continuous geomagnetic field data in an earthquake zone to look for indications of anomalous changes in 683  
fractal dimensions, which may indicate the effect of occurrence of an earthquake. So far the results have 684  
shown promise, but not yet yielded definitive correlations, a clear argument that many more and systematic 685  
studies are required. 686

Fractal analysis of geomagnetic signals has revealed varying patterns and amplitudes of fractal dimensions 687  
representing seismo-electromagnetic (SEM) signatures. The amplitude of enhanced fractal dimension 688  
observed by Hayakawa et al. (1999), for a magnitude 8 earthquake is approximately 10 times higher than 689  
the fractal dimension observed in our study (for earthquakes of magnitude 4.5-5.1). While enhancements 690  
from both studies are linked to microfracturing processes, the variation in amplitude creates ambiguity in 691  
connecting parameters such as physical properties of the medium (conductivity, permeability, elastic 692  
modulus, etc.), scale of microfracturing, earthquake characteristics (epicentral distance, magnitude, and 693  
focal depth), and the method used for computing fractal dimension. Gotoh et al. (2003) observed high 694  
fractal dimension values from the H-component (in the noon sector, i.e., 12:00-13:00 LT) as signatures of 695  
an earthquake swarm, whereas in our study we found signatures in multifractal parameters of the Z- 696  
component (night sector 22:00-02:00 LT). Thus, the fractal dimension shows different results depending on 697  
the data component (H or Z) and time of day (day or night) when characterizing similar earthquake events. 698  
Ida et al. (2012) observed a decrease in the fractal dimension of the Z-component as a seismic precursor to 699  
major earthquakes. This observation contrasts with findings from the 2003 Guam and 2000 Izu Islands 700  
earthquake swarms, as well as our studies, which noted an increase in fractal dimension before earthquakes. 701  
Ida et al. (2012) suggested that this discrepancy might stem from different dominant processes: inland pre- 702  
earthquake activity could be characterized by low-frequency electrokinetic processes, while oceanic 703  
activity might be dominated by high-frequency microfracturing processes. It should also be kept in mind 704  
that in the tropical regions, any diurnal variation in the atmospheric electrical potential will be more 705  
effective to change the electrical current flowing to the Earth's subsurface compared with higher latitudes. 706  
Consequently, tectonic faults here can experience greater electrical currents, as increased porosity and 707  
micro-fractures make them good conductors. These effects are likely to have a much stronger effect on the 708

Z component of the geomagnetic field at lower latitudes. Moreover, earthquake catalogs for moderate- 709  
magnitude events may offer less precise parameters, such as magnitude, hypocenter, and focal depth. This 710  
imprecision can lead to misinterpretation of fractal dimension results in the context of seismo- 711  
electromagnetic (SEM) signatures. Thus, interpretations of fractal variations of geomagnetic field data need 712  
to be made in the context of earthquake magnitudes and focal depths, focal mechanisms and triggering 713  
phenomena, location of the active faults, the distance of the geomagnetic recording station and length of 714  
data available, as well as associated EM signatures like TEC changes and radon emissions in a systematic 715  
manner, which demand further in-depth study to resolve the ambiguities. 716

We have defined four clusters of the earthquakes under study (1-45, 47-48, 50-51, 53-55). There are 10 717  
earthquakes, which occurred as single events. For the single events 52, 56-63 ( $4.5 < M < 5.0$ ), which are 718  
characterized by either large focal depth ( $>100$  km) or large epicentral distance ( $\sim 200$  km), signatures in 719  
multifractal parameters. We infer that the EM fields from such moderate magnitude and large epicentral 720  
distance earthquakes are too weak to detect by multifractal and diurnal ratio approach (Prajapati and Arora., 721  
under review). For the same single events (with focal depth  $>100$ km or epicentral distance  $\sim 200$  km), we 722  
observed that enhancements in  $f_D$  corresponding to earthquakes 56,57,58, 60, and 61 while the earthquake 723  
52, 59, 62, 63 are not correspond to any pre-co or post enhancements in  $f_D$  parameter. The significant 724  
enhancement corresponds to 5 events out of 9, including two co-seismic signature (60 and 61) indicate the 725  
greater efficacy of  $f_D$  parameter than multifractal parameter for single events with focal depth  $>100$ km or 726  
epicentral distance  $\sim 200$  km. The earthquake 52 is associated with an increase in the Diurnal ratio 13 days 727  
in advance. The single event 49 is characterized by moderate focal depth and epicentral distance, which is 728  
associated with co-seismic enhancements in  $f_D$ , pre-seismic signatures in  $h_w$  (7 days prior) and diurnal 729  
ratio (15 days prior). 730

The clusters, on the other hand, produce prominent signatures in the multifractal parameters. The first cluster (1-45) has signature in  $h_w$  (14 days prior) and a co-seismic enhancement in  $f_{max}$ . The second cluster (47-48) has signatures in  $f_{max}$ ,  $h_{max}$  and diurnal ratio, 9, 9, 13 days prior to event respectively. The third cluster (50-51) at a larger epicentral distance of 165 km, has signatures in  $f_D$ ,  $h_w$  and diurnal ratio 19, 9, 19 days prior to event respectively. The fourth cluster (53-55) includes earthquakes of  $M=5.1$  and the events are at shallow focal depth and small-to-moderate epicentral distances produce signatures in  $f_D$  and all the multifractal parameters as well as diurnal ratio.

The combined observation from fractal (mono and multifractal) and diurnal ratio (Table 1) clearly indicates that the fractal parameters exhibit significant enhancement associated with 10 earthquakes (including co-seismic signatures), while significant enhancements in diurnal ratio are correlated with nine earthquakes out of ten (including two post-seismic signatures).

**Table 1:** The following table summarizes the earthquake and its characteristics presence (Y) or absence (-) of potential enhancements in monofractal ( $f_D$ ) and multifractal ( $h_w, f_{max}, h_{max}$ ) components and diurnal ratio.

EQ. No.	Magnitude	Focal Depth (Km)	Epicentral Distance (Km)	Single /Cluster (S) (C)	$f_D$	$h_w$	$f_{max}$	$h_{max}$	Diurnal ratio
1-45	-	Moderate	Moderate	C	-	Y	Co-	-	-
46-48	Moderate	Moderate	Moderate	C	-	-	Y	Y	Y
49	Moderate	Moderate	Moderate	S	Co-	Y	-	-	Y
50-51	Moderate	Shallow/ Large	Large	C	Y	Y	-	-	Post-
52	Moderate	Shallow	Large	S	-	-	-	-	Y
53-54- 55	Large	Shallow	Small	C	Y	Y	Y	Y	Y

56	Moderate	Moderate	Large	S	Y	-	-	-	-
57	Large	Shallow	Large	S	Y	-	-	-	-
58	Large	Large	Mod	S	Y	-	-	-	-
59	Moderate	Shallow	Large	S	-	-	-	-	Y
60	Moderate	Large	Moderate	S	Co-	-	-	-	Y
61	Moderate	Shallow	Large	S	Co-	-	-	-	Y
62	Moderate	Shallow	Large	S	-	-	-	-	-
63	Moderate	Shallow	Large	S	-	-	-	-	post

According to Ida et al. (2012), significant enhancements in fractal values of geomagnetic signal recorded 745  
in tectonic active areas are representing the dominance of high frequency component associated with EM 746  
field from microfracturing processes in lithosphere. Apart from this, the components of holder exponent 747  
(part of multifractal analysis) such as  $f_{max}$ ,  $h_{max}$ ,  $h_{min}$ , and  $h(0)$  also analyses the different characteristics 748  
of the signal (Krzyszczak et al., 2019) such as enhancement in  $h_{max}$  indicates that underlying process of 749  
events are more smooth rather than sorter fluctuations while  $h_{min}$  is just opposite to  $h_{max}$ . Similarly,  $f_{max}$  750  
is correspond to  $h(0)$  i.e.  $h$  which occurred maximum number of times in range  $h_{max}$ -  $h_{min}$ . The 751  
enhancements in  $f_{max}$  value with large  $h$  indicate the underlying processes is less correlated and fine 752  
structure i.e. signal embedded with anomalies and not completely regular while  $f_{max}$  correspond to smaller 753  
value of  $h$  indicate the highly correlated and most regular signal. Enhancements in  $h_{max}$  and  $f_{max}$  with  $h(0)$  754  
correspond to large  $h$  of a geomagnetic signal recorded in active tectonic area, indicates that the underlying 755  
processes is smooth and exhibit anomalies (less correlated and fine structures) of low frequencies. 756  
According to Conti et al. (2021) electrokinetic process is responsible for generation of low frequency EM 757  
signature from lithospheric deformation of a focal zone. 758

The enhancements in  $h_{max}$  and  $f_{max}$ , preceding the clusters of shallow earthquakes 1-45, 46-48, 53-55 on 759  
the SS fault at moderate epicentral distances are indicative of low frequency perturbations from multiple 760

sources, which are ascribed to electrokinetic processes (Conti et al., 2021). For the cluster 50-51, the former 761  
occurs on the SS fault and the latter on the WAF leading to interferences of the EM signals, whereby the 762  
 $h_{max}$  and  $f_{max}$  763  
enhancements are not prominent. 764

The earthquakes 49, 51 and 52 on the WAF dominated by strike slip mechanisms are also shallow and are 765  
at moderate epicentral distances but have enhancements in  $f_D$  and  $h_w$ , the latter being more significant. 766  
This is interpreted as high frequency perturbations attributed to microfracturing processes (Ida et al., 2012). 767  
The earthquakes 56, 57, 59, 60, 61, 63 on the WAF and AT faults at large epicentral distances are linked 768  
with enhancements in  $f_D$  and  $h_w$ , the former being more significant. We interpret these high frequency 769  
perturbations to be also generated due to microfracturing processes; the large epicentral distances possibly 770  
leading to attenuation of the highest frequency components leads to more prominent monofractal 771  
signatures. The earthquakes 50, 58 and 62 are either at very large epicentral distances or large focal depths 772  
and fail to produce signatures in any of the fractal components. 773

Thus, the moderate focal depth and epicenter distance earthquakes on WAF are dominated by  $h_w$  while 774  
large focal depth and epicentre distance earthquakes on WAF/AT dominated by  $f_D$  possibly indicating that 775  
the EM field from large distance are more homogeneous due to attenuation and dominating its appearance 776  
in  $f_D$  component, while EM field from short distance, indicating that EM field are more heterogeneous and 777  
dominating its appearance in  $h_w$  component. Which means,  $f_D$  component is most sensitive component for 778  
large epicenter and focal depth earthquakes while  $h_w$  component is more sensitive for moderate epicentre 779  
distance and focal depth earthquakes. 780

## 5. Conclusions 781

The study of fractal natures of the geomagnetic time series (Z component) allows us to conclude: 782

- (i) The earthquake clusters occurred on normal/thrust fault are of moderate magnitude and focal depth 783  
are emitting prior EM fields of low frequency effectively generated from electrokinetic processes 784  
in focal zone of earthquake. 785
- (ii) The single earthquakes occurred on strike slip WAF fault of moderate magnitude and focal depth 786  
are emitting prior EM field of more heterogeneity and frequency while, earthquakes on same fault 787  
with large epicentre distance/ focal depth emitting prior EM field of lesser heterogeneity and high 788  
frequency effectively generated from microfracturing processes in focal zone of earthquake. 789
- (iii) The monofractal dimension  $f_D$  is more effective to trace the EM field from large epicentre distance 790  
and focal depth while multifractal spectrum width  $h_w$  is more effective to trace the EM field from 791  
moderate to small epicentre distance and focal depth for the case of microfracturing processes. 792
- (iv) The fractal analysis has advantage over diurnal ratio is simultaneous observation of high and low 793  
frequency EM field from lithospheric deformation of focal zone of earthquake, which are emitted 794  
from different pre-earthquake processes. 795

## Statements and Declarations 796

### (i) Data Availability 797

The data that support the findings of this study are available upon reasonable request. 798  
799

### (ii) Competing Interests 801

The authors have no relevant financial or non-financial interests to disclose. 802  
803

### (iii) CRediT authorship contribution statement 805

All authors contributed to the study conception and design. Methodology and data collection 806  
were performed by Kusumita Arora, and Rahul Prajapati. Data curation and its analysis using 807  
MATLAB coding was performed by Rahul Prajapati. The first draft of the manuscript was 808  
written by Rahul Prajapati. Review and editing of first draft of the manuscript performed by 809  
810



Kusumita Arora, and the work carried out under supervision and validation of Kusumita Arora. 811  
All authors read and approved the final manuscript. 812

813

**Acknowledgments:** The Authors are thankful to the Director CSIR-National Geophysical Research 814  
Institute, India for granting permission to access the data for research purpose and to publish the work 815  
(Ref. No. NGRI/Lib/2024/Pub-019). The authors acknowledge the available public domain data sets 816  
from WDC Kyoto (<https://wdc.kugi.kyoto-u.ac.jp/>) and earthquake data from ISC catalogue 817  
(<http://www.isc.ac.uk/iscbulletin/search/catalogue/>). Authors are also acknowledging the Dr. N. Phani 818  
Chandrasekhar and other observatories staff for maintaining the remote site observatories to acquire the 819  
uninterrupted data. 820

821

## References 822

Babu, S. S. and Unnikrishnan, K.: Analysis of fractal properties of horizontal component of Earth's 823  
magnetic field of different geomagnetic conditions using MFDFA, *Adv. Sp. Res.*, 72, 2391–2405, 2023. 824

825

Bak, P., Tang, C., and Wiesenfeld, K.: Self-organized criticality, *Phys. Rev. A*, 38, 364, 1988. 826

Barnsley, M. F., Elton, J., Hardin, D., and Massopust, P.: Hidden variable fractal interpolation functions, 827  
*SIAM J. Math. Anal.*, 20, 1218–1242, 1989. 828

Barabási, A.-L. and Vicsek, T.: Multifractality of self-affine fractals, *Phys. Rev. A*, 44, 2730, 1991. 829

Borovsky, J. E.: Magnetospheric plasma systems science and solar wind plasma systems science: The 830  
plasma-wave interactions of multiple particle populations, *Front. Astron. Sp. Sci.*, 8, 780321, 2021. 831

Bella, J., Brodsky, B., and Berman, H. M.: Hydration structure of a collagen peptide, *Structure*, 3, 893– 832  
906, 1995. 833

Bhattacharya, K. and Manna, S. S.: Self-organized critical models of earthquakes, *Phys. A Stat. Mech. its 834  
Appl.*, 384, 15–20, 2007. 835

Bulusu, J., Arora, K., Singh, S., and Edara, A.: Simultaneous electric, magnetic and ULF anomalies 836  
associated with moderate earthquakes in Kumaun Himalaya, *Nat. Hazards*, 1–31, 2023. 837

Borovsky, J. E. and Valdivia, J. A.: The Earth's magnetosphere: a systems science overview and assessment, *Surv. Geophys.*, 39, 817–859, 2018. 838  
839

Chadha, R. K., Singh, C., and Shekar, M.: Transient changes in well-water level in bore wells in Western India due to the 2004 M W 9.3 Sumatra Earthquake, *Bull. Seismol. Soc. Am.*, 98, 2553–2558, 2008. 840  
841

Chen, C. C., Wang, W. C., Chang, Y. F., Wu, Y. M., and Lee, Y. H.: A correlation between the b-value and the fractal dimension from the aftershock sequence of the 1999 Chi-Chi, Taiwan, earthquake, *Geophys. J. Int.*, 167, 1215–1219, <https://doi.org/10.1111/j.1365-246X.2006.03230.x>, 2006. 842  
843  
844

Chen, Y.: Characterizing growth and form of fractal cities with allometric scaling exponents, *Discret. Dyn. Nat. Soc.*, 2010, <https://doi.org/10.1155/2010/194715>, 2010. 845  
846

Chen, Y. and Zhou, Y.: Scaling laws and indications of self-organized criticality in urban systems, *Chaos, Solitons and Fractals*, 35, 85–98, <https://doi.org/10.1016/j.chaos.2006.05.018>, 2008. 847  
848  
849

Conti, L., Picozza, P., and Sotgiu, A.: A critical review of ground based observations of earthquake precursors, *Front. Earth Sci.*, 9, 676766, 2021. 850  
851

Currenti, G., Del Negro, C., Lapenna, V., and Telesca, L.: Natural Hazards and Earth System Sciences Multifractality in local geomagnetic field at Etna volcano, Sicily (southern Italy), *Natural Hazards and Earth System Sciences*, 555–559 pp., 2005. 852  
853  
854  
855

Crampin, S., McGonigle, R., and Bamford, D.: Estimating crack parameters from observations of P-wave velocity anisotropy, *Geophysics*, 45, 345–360, 1980. 856  
857

Currenti, G., Del Negro, C., Lapenna, V., and Telesca, L.: Multifractality in local geomagnetic field at Etna volcano, Sicily (southern Italy), *Nat. Hazards Earth Syst. Sci.*, 5, 555–559, 2005. 858  
859

Dimri, V. P.: *Fractal behaviour of the earth system*, Springer, 2005. 860

El-Nabulsi, R. A. and Anukool, W.: Time-dependent heating problem of the solar corona in fractal dimensions: A plausible solution, *Adv. Sp. Res.*, 74, 2510–2529, <https://doi.org/10.1016/j.asr.2024.06.015>, 2024. 861  
862  
863

Fraser-Smith, A. C., Bernardi, A., McGill, P. R., Ladd, M., Helliwell, R. A., and Villard Jr, O. G.: Low-frequency magnetic field measurements near the epicenter of the Ms 7.1 Loma Prieta earthquake, *Geophys. Res. Lett.*, 17, 1465–1468, 1990. 864  
865  
866

Freund, F. and Sornette, D.: Electro-magnetic earthquake bursts and critical rupture of peroxy bond 867

networks in rocks, *Tectonophysics*, 431, 33–47, 2007. 868

Gahalaut, V. K., Kundu, B., Laishram, S. S., Catherine, J., Kumar, A., Singh, M. D., Tiwari, R. P., Chadha, R. K., Samanta, S. K., and Ambikapathy, A.: Aseismic plate boundary in the Indo-Burmese wedge, northwest Sunda Arc, *Geology*, 41, 235–238, 2013. 869  
870  
871

Gao, X.-Y., Guo, Y.-J., and Shan, W.-R.: Optical waves/modes in a multicomponent inhomogeneous optical fiber via a three-coupled variable-coefficient nonlinear Schrödinger system, *Appl. Math. Lett.*, 120, 107161, 2021. 872  
873  
874

Godano, C., Alonzo, M. L., and Bottari, A.: Multifractal analysis of the spatial distribution of earthquakes in southern Italy, *Geophys. J. Int.*, 125, 901–911, <https://doi.org/10.1111/j.1365-246X.1996.tb06033.x>, 1996. 875  
876  
877

Gong, P. and Howarth, P. J.: The use of structural information for improving land-cover classification accuracies at the rural-urban fringe, *Photogramm. Eng. Remote Sens.*, 1990. 878  
879

Gotoh, K., Akinaga, Y., Hayakawa, M., and Hattori, K.: Principal component analysis of ULF geomagnetic data for Izu islands earthquakes in July 2000, *J. Atmos. Electr.*, 22, 1–12, 2002. 880  
881

Gotoh, K., Hayakawa, M., and Smirnova, N.: Fractal analysis of the ULF geomagnetic data obtained at Izu Peninsula, Japan in relation to the nearby earthquake swarm of, *Natural Hazards and Earth System Sciences*, 229–236 pp., 2003. 882  
883  
884

Gotoh, K., Hayakawa, M., Smirnova, N. A., and Hattori, K.: Fractal analysis of seismogenic ULF emissions, *Phys. Chem. Earth, Parts A/B/C*, 29, 419–424, 2004. 885  
886

Gvozdarev, A. and Parovik, R.: On the Relationship between the Fractal Dimension of Geomagnetic Variations at Altay and the Space Weather Characteristics, *Mathematics*, 11, 3449, <https://doi.org/10.3390/math11163449>, 2023. 887  
888  
889

Han, P., Hattori, K., Xu, G., Ashida, R., Chen, C.-H., Febriani, F., and Yamaguchi, H.: Further investigations of geomagnetic diurnal variations associated with the 2011 off the Pacific coast of Tohoku earthquake (Mw 9.0), *J. Asian Earth Sci.*, 114, 321–326, 2015. 890  
891  
892

Han, P., Hattori, K., Huang, Q., Hirooka, S., and Yoshino, C.: Spatiotemporal characteristics of the geomagnetic diurnal variation anomalies prior to the 2011 Tohoku earthquake (Mw 9.0) and the possible coupling of multiple pre-earthquake phenomena, *J. Asian Earth Sci.*, 129, 13–21, 2016. 893  
894  
895

Haralick, R. M., Shanmugam, K., and Dinstein, I. H.: Textural features for image classification, *IEEE Trans. Syst. Man. Cybern.*, 610–621, 1973. 896  
897

Harris, S. K.: NATIONAL CENTER FOR EARTHQUAKE The Island of Guam Earthquake of, 1993. 898

Hattori, K., Serita, A., Gotoh, K., Yoshino, C., Harada, M., Isezaki, N., and Hayakawa, M.: ULF geomagnetic anomaly associated with 2000 Izu islands earthquake swarm, Japan, *Phys. Chem. Earth, Parts* 899  
900

A/B/C, 29, 425–435, 2004a. 901

Hattori, K., Takahashi, I., Yoshino, C., Isezaki, N., Iwasaki, H., Harada, M., Kawabata, K., Kopytenko, E., Kopytenko, Y., Maltsev, P., Korepanov, V., Molchanov, O., Hayakawa, M., Noda, Y., Nagao, T., and Uyeda, S.: ULF geomagnetic field measurements in Japan and some recent results associated with Iwateken Nairiku Hokubu earthquake in 1998, *Phys. Chem. Earth*, 29, 481–494, <https://doi.org/10.1016/j.pce.2003.09.019>, 2004b. 902  
903  
904  
905  
906

Hattori, K.: ULF geomagnetic changes associated with large earthquakes, *Terr. Atmos. Ocean. Sci.*, 15, 329–360, 2004. 907  
908

Hayakawa, M., Ito, T., and Smirnova, N.: Fractal analysis of ULF geomagnetic data associated with the Guam earthquake on August 8, 1993, *Geophys. Res. Lett.*, 26, 2797–2800, <https://doi.org/10.1029/1999GL005367>, 1999. 909  
910  
911

Hayakawa, M., Itoh, T., Hattori, K., and Yumoto, K.: ULF electromagnetic precursors for an earthquake at Biak, Indonesia on February 17, 1996, *Geophys. Res. Lett.*, 27, 1531–1534, <https://doi.org/10.1029/1999GL005432>, 2000. 912  
913  
914

Hayat, U., Barkat, A., Ali, A., Rehman, K., Sifat, S., and Iqbal, T.: Fractal analysis of shallow and intermediate-depth seismicity of Hindu Kush, *Chaos, Solitons and Fractals*, 128, 71–82, <https://doi.org/10.1016/j.chaos.2019.07.029>, 2019. 915  
916  
917

Hattori, K., Han, P., Yoshino, C., Febriani, F., Yamaguchi, H., and Chen, C. H.: Investigation of ULF Seismo-Magnetic Phenomena in Kanto, Japan During 2000-2010: Case Studies and Statistical Studies, <https://doi.org/10.1007/s10712-012-9215-x>, 1 May 2013a. 918  
919  
920

Hattori, K., Han, P., Yoshino, C., Febriani, F., Yamaguchi, H., and Chen, C.-H.: Investigation of ULF seismo-magnetic phenomena in Kanto, Japan during 2000–2010: case studies and statistical studies, *Surv. Geophys.*, 34, 293–316, 2013b. 921  
922  
923

Hayakawa, M. and Molchanov, O. A.: Summary report of NASDA’s earthquake remote sensing frontier project, *Phys. Chem. Earth, Parts A/B/C*, 29, 617–625, 2004. 924  
925

Hayakawa, M., Kawate, R., Molchanov, O. A., and Yumoto, K.: Results of ultra-low-frequency magnetic field measurements during the Guam earthquake of 8 August 1993, *Geophys. Res. Lett.*, 23, 241–244, 1996. 926  
927  
928

Hayakawa, M., Ito, T., and Smirnova, N.: Fractal analysis of ULF geomagnetic data associated with the Guam earthquake on August 8, 1993, *Geophys. Res. Lett.*, 26, 2797–2800, <https://doi.org/10.1029/1999GL005367>, 1999. 929  
930  
931

Hayakawa, M., Itoh, T., Hattori, K., and Yumoto, K.: ULF electromagnetic precursors for an earthquake at Biak, Indonesia on February 17, 1996, *Geophys. Res. Lett.*, 27, 1531–1534, 2000. 932  
933

Hayakawa, M., Ida, Y. U. I., and Gotoh, K.: Multifractal analysis for the ULF geomagnetic data during the Guam earthquake, in: IEEE 6th International Symposium on Electromagnetic Compatibility and Electromagnetic Ecology, 2005, Proceedings, 239–243, <https://doi.org/10.1109/EMCECO.2005.1513113>, 2005. 934–937

Hayakawa, M., Hattori, K., and Ohta, K.: Monitoring of ULF (ultra-low-frequency) Geomagnetic Variations Associated with Earthquakes, *Sensors*, 7, 1108–1122, 2007. 938–939

He, P., Wen, Y., Xu, C., Liu, Y., and Fok, H. S.: New Evidence for Active Tectonics at the Boundary of the Kashi Depression, China, from Time Series InSAR Observations *Tectonophysics* New evidence for active tectonics at the boundary of the Kashi Depression, China, from time series InSAR observations, *Tectonophysics*, 653, 140–148, <https://doi.org/10.1016/j.tecto.2015.04.011>, 2015. 940–943

Heavlin, W. D., Kappler, K., Yang, L., Fan, M., Hickey, J., Lemon, J., MacLean, L., Bleier, T., Riley, P., and Schneider, D.: Case-Control Study on a Decade of Ground-Based Magnetometers in California Reveals Modest Signal 24–72 hr Prior to Earthquakes, *J. Geophys. Res. Solid Earth*, 127, <https://doi.org/10.1029/2022JB024109>, 2022. 944–947

Higuchi, T.: Approach to an irregular time series on the basis of the fractal theory, *Phys. D Nonlinear Phenom.*, 31, 277–283, 1988. 948–949

Hirata, T. and Imoto, M.: Multifractal analysis of spatial distribution of microearthquakes in the Kanto region, *Geophys. J. Int.*, 107, 155–162, 1991. 950–951

Ida, Y., Hayakawa, M., Adalev, A., and Gotoh, K.: Multifractal analysis for the ULF geomagnetic data during the 1993 Guam earthquake, *Nonlinear Process. Geophys.*, 12, 157–162, <https://doi.org/10.5194/npg-12-157-2005>, 2005. 952–954

Ida, Y., Yang, D., Li, Q., Sun, H., and Hayakawa, M.: Detection of ULF electromagnetic emissions as a precursor to an earthquake in China with an improved polarization analysis, *Hazards Earth Syst. Sci*, 775–777 pp., 2008. 955–957

Ida, Y., Yang, D., Li, Q., Sun, H., and Hayakawa, M.: Fractal analysis of ULF electromagnetic emissions in possible association with earthquakes in China, *Nonlinear Process. Geophys.*, 19, 577–583, <https://doi.org/10.5194/npg-19-577-2012>, 2012. 958–960

Jacquin, A. E.: Fractal image coding: A review, *Proc. IEEE*, 81, 1451–1465, 1993. 961

Jaffard, S., Lashermes, B., and Abry, P.: Wavelet leaders in multifractal analysis, *Wavelet Anal. Appl.*, 1, 219–264, 2006. 962–963

Johnston, M. J. S., Mueller, R. J., Ware, R. H., and Davis, P. M.: Precision of geomagnetic field measurements in a tectonically active region, *J. Geomagn. Geoelectr.*, 36, 83–95, 1984. 964–965

Kagan, Y. Y. and Knopoff, L.: Spatial distribution of earthquakes: the two-point correlation function, 966

Geophys. J. Int., 62, 303–320, 1980.	967
Kantelhardt, J. W., Zschiegner, S. A., Koscielny-Bunde, E., Havlin, S., Bunde, A., and Stanley, H. E.: Multifractal detrended fluctuation analysis of nonstationary time series, Phys. A Stat. Mech. its Appl., 316, 87–114, 2002.	968 969 970
Keersmaecker, De. M. L., Frankhauser, P., and Thomas, I.: Using fractal dimensions for characterizing intra-urban diversity: The example of Brussels, Geogr. Anal., 35, 310–328, <a href="https://doi.org/10.1111/j.1538-4632.2003.tb01117.x">https://doi.org/10.1111/j.1538-4632.2003.tb01117.x</a> , 2003.	971 972 973
Kiyashchenko, D., Smirnova, N., Troyan, V., and Vallianatos, F.: Dynamics of multifractal and correlation characteristics of the spatio-temporal distribution of regional seismicity before the strong earthquakes, Natural Hazards and Earth System Sciences, 285–298 pp., 2003.	974 975 976
Koizumi, N., Kitagawa, Y., Matsumoto, N., Takahashi, M., Sato, T., Kamigaichi, O., and Nakamura, K.: Preseismic groundwater level changes induced by crustal deformations related to earthquake swarms off the east coast of Izu Peninsula, Japan, Geophys. Res. Lett., 31, 2004.	977 978 979
Kopytenko, Y. A., Matiashvili, T. G., Voronov, P. M., Kopytenko, E. A., and Molchanov, O. A.: Detection of ultra-low-frequency emissions connected with the Spitak earthquake and its aftershock activity, based on geomagnetic pulsations data at Dusheti and Vardzia observatories, Phys. Earth Planet. Inter., 77, 85–95, 1993.	980 981 982 983
Krzyszczak, J., Baranowski, P., Zubik, M., Kazandjiev, V., Georgieva, V., Cezary, S., Siwek, K., Kozyra, J., and Nieróbca, A.: Multifractal characterization and comparison of meteorological time series from two climatic zones, 1811–1824, 2019.	984 985 986
Lashermes, B., Jaffard, S., and Abry, P.: Wavelet leader based multifractal analysis, in: Proceedings.(ICASSP'05). IEEE International Conference on Acoustics, Speech, and Signal Processing, 2005., iv–161, 2005.	987 988 989
Liebovitch, L. S. and Toth, T.: A fast algorithm to determine fractal dimensions by box counting, Phys. Lett. A, 141, 386–390, 1989.	990 991 992
Liu, J. Y., Tsai, Y. B., Chen, S. W., Lee, C. P., Chen, Y. C., Yen, H. Y., Chang, W. Y., and Liu, C.: Giant ionospheric disturbances excited by the M9.3 Sumatra earthquake of 26 December 2004, Geophys. Res. Lett., 33, 2006.	993 994 995
Lopes, R. and Betrouni, N.: Fractal and multifractal analysis: a review, Med. Image Anal., 13, 634–649, 2009.	996 997
López-Casado, C., Henares, J., Badal, J., and Peláez, J. A.: Multifractal images of the seismicity in the	998

Ibero-Maghrebian region (westernmost boundary between the Eurasian and African plates), 999  
Tectonophysics, 627, 82–97, <https://doi.org/10.1016/j.tecto.2013.11.013>, 2014. 1000

Mandal, P., Mabawonku, A. O., and Dimri, V. P.: Self-organized fractal seismicity of reservoir triggered 1001  
earthquakes in the Koyna-Warna seismic zone, Western India, Pure Appl. Geophys., 162, 73–90, 1002  
<https://doi.org/10.1007/s00024-004-2580-8>, 2005. 1003  
1004

Mandelbrot, B. B. and Van Ness, J. W.: Fractional Brownian motions, fractional noises and applications, 1005  
SIAM Rev., 10, 422–437, 1968. 1006

Mandelbrot, B. B.: Fractals, Form, chance Dimens., 1977. 1007

Mandelbrot, B. B.: Multifractal measures, especially for the geophysicist, Fractals Geophys., 5–42, 1989. 1008

Mandelbrot, B. B. and Mandelbrot, B. B.: The fractal geometry of nature, WH freeman New York, 1982. 1009

Meng, J., Wang, C., Zhao, X., Coe, R., Li, Y., and Finn, D.: India-Asia collision was at 24 N and 50 Ma: 1010  
palaeomagnetic proof from southernmost Asia, Sci. Rep., 2, 925, 2012. 1011

Molchan, G. and Kronrod, T.: The fractal description of seismicity, Geophys. J. Int., 179, 1787–1799, 1012  
<https://doi.org/10.1111/j.1365-246X.2009.04380.x>, 2009. 1013

Molchanov, O. A. and Hayakawa, M.: Generation of ULF electromagnetic emissions by microfracturing, 1014  
Geophys. Res. Lett., 22, 3091–3094, <https://doi.org/10.1029/95GL00781>, 1995. 1015

Molchanov, O. A., Kopytenko, Y. A., Voronov, P. M., Kopytenko, E. A., Matiashvili, T. G., Fraser-Smith, 1016  
A. C., and Bernardi, A.: Results of ULF magnetic field measurements near the epicenters of the Spitak 1017  
(Ms= 6.9) and Loma Prieta (Ms= 7.1) earthquakes: Comparative analysis, Geophys. Res. Lett., 19, 1495– 1018  
1498, 1992. 1019

Muzy, J.-F., Bacry, E., and Arneodo, A.: The multifractal formalism revisited with wavelets, Int. J. Bifurc. 1020  
Chaos, 4, 245–302, 1994. 1021

Myint, S. W.: Fractal approaches in texture analysis and classification of remotely sensed data: 1022  
Comparisons with spatial autocorrelation techniques and simple descriptive statistics, Int. J. Remote Sens., 1023  
24, 1925–1947, 2003. 1024  
1025

Ouzounov, D., Liu, D., Chunli, K., Cervone, G., Kafatos, M., and Taylor, P.: Outgoing long wave radiation 1026  
variability from IR satellite data prior to major earthquakes, Tectonophysics, 431, 211–220, 2007. 1027

Panda, M. N., Mosher, C., and Chopra, A. K.: Application of wavelet transforms to reservoir data analysis 1028  
and scaling, in: SPE Annual Technical Conference and Exhibition, 1996. 1029

Panda, S. K., Choudhury, S., Saraf, A. K., and Das, J. D.: MODIS land surface temperature data detects thermal anomaly preceding 8 October 2005 Kashmir earthquake, *Int. J. Remote Sens.*, 28, 4587–4596, 2007. 1030  
1031  
1032

Pastén, D. and Pavez-Orrego, C.: Multifractal time evolution for intraplate earthquakes recorded in southern Norway during 1980–2021, *Chaos, Solitons & Fractals*, 167, 113000, 2023. 1033  
1034

Pentland, A. P.: Fractal-based description of natural scenes, *IEEE Trans. Pattern Anal. Mach. Intell.*, 661–674, 1984. 1035  
1036

Prajapati, R., Arora, A.: Investigation of geomagnetic field variations in search of seismo-electromagnetic emissions associated with earthquakes in subduction zone of Andaman-Nicobar, India, 2023. 1037  
1038  
1039

Potirakis, S. M., Hayakawa, M., and Schekotov, A.: Fractal analysis of the ground-recorded ULF magnetic fields prior to the 11 March 2011 Tohoku earthquake ( $M_W = 9$ ): discriminating possible earthquake precursors from space-sourced disturbances, *Nat. Hazards*, 85, 59–86, <https://doi.org/10.1007/s11069-016-2558-8>, 2017. 1040  
1041  
1042  
1043

Qiuming, C.: Fractal density and singularity analysis of heat flow over ocean ridges, *Sci. Rep.*, 6, 1–10, <https://doi.org/10.1038/srep19167>, 2016. 1044  
1045

Rahimi-Majd, M., Shirzad, T., and Najafi, M. N.: A self-organized critical model and multifractal analysis for earthquakes in Central Alborz, Iran, *Sci. Rep.*, 12, 8364, 2022. 1046  
1047

Rawat, G., Chauhan, V., and Dhamodharan, S.: Fractal dimension variability in ULF magnetic field with reference to local earthquakes at MPMO, Ghuttu, Geomatics, *Nat. Hazards Risk*, 7, 1937–1947, <https://doi.org/10.1080/19475705.2015.1137242>, 2016. 1048  
1049  
1050

Rossi, G.: Fractal analysis as a tool to detect seismic cycle phases, in: *Fractals and Dynamic Systems in Geoscience*, Springer, 169–179, 1994. 1051  
1052

Roy, P. N. S. and Mondal, S. K.: Multifractal analysis of earthquakes in Kumaun Himalaya and its surrounding region, *Journal of earth system science.*, 121, 1033-1047, 2012. 1053  
1054

Rikitake, T.: Earthquake precursors, *Bull. Seismol. Soc. Am.*, 65, 1133–1162, 1975. 1055

Schaefer, D. W.: Fractal models and the structure of materials, *MRS Bull.*, 13, 22–27, 1988. 1056

Scholz, C. H., Sykes, L. R., and Aggarwal, Y. P.: Earthquake Prediction: A Physical Basis: Rock dilatancy and water diffusion may explain a large class of phenomena precursory to earthquakes., *Science (80-. )*, 181, 803–810, 1973. 1057  
1058  
1059

Serrano, E. and Figliola, A.: Wavelet Leaders: A new method to estimate the multifractal singularity spectra, *Phys. A Stat. Mech. its Appl.*, 388, 2793–2805, <https://doi.org/10.1016/j.physa.2009.03.043>, 2009. 1060  
1061  
1062

Sethumadhav, M. S., Gunnell, Y., Ahmed, M. M., and Chinnaiyah: Late Archean manganese mineralization 1063



- and younger supergene manganese ores in the Anmod-Bisgod region, Western Dharwar Craton, southern India: Geological characterization, palaeoenvironmental history, and geomorphological setting, *Ore Geol. Rev.*, 38, 70–89, <https://doi.org/10.1016/j.oregeorev.2010.06.001>, 2010. 1064  
1065  
1066
- Shen, Y. and Tian, B.: Bilinear auto-Bäcklund transformations and soliton solutions of a (3+ 1)-dimensional generalized nonlinear evolution equation for the shallow water waves, *Appl. Math. Lett.*, 122, 107301, 2021. 1067  
1068  
1069
- Smirnova, N., Hayakawa, M., and Gotoh, K.: Precursory behavior of fractal characteristics of the ULF electromagnetic fields in seismic active zones before strong earthquakes, *Phys. Chem. Earth, Parts A/B/C*, 29, 445–451, 2004. 1070  
1071  
1072
- Smirnova, N. A., Kiyashchenko, D. A., Troyan, V. N., and Hayakawa, M.: Multifractal Approach to Study the Earthquake Precursory Signatures Using the Ground-Based Observations, *Review of Applied Physics*, Hayakawa and Ida, 2013. 1073  
1074  
1075
- Sridharan, M. and Ramasamy, A. M. S.: Fractal analysis for geomagnetic secular variations, *J. Indian Geophys. Union*, 10, 175–185, 2006. 1076  
1077
- Stanica, D. A. and Stănică, D.: ULF pre-seismic geomagnetic anomalous signal related to Mw8.1 offshore chiapas earthquake, Mexico on 8 September 2017, *Entropy*, 21, <https://doi.org/10.3390/e21010029>, 2019. 1078  
1079
- Szczepaniak, A. and Macek, W. M.: Asymmetric multifractal model for solar wind intermittent turbulence, *Nonlinear Process. Geophys.*, 15, 615–620, 2008. 1080  
1081
- Telesca, L., Colangelo, G., Lapenna, V., and Macchiato, M.: Monofractal and multifractal characterization of geoelectrical signals measured in southern Italy, *Chaos, Solitons and Fractals*, 18, 385–399, [https://doi.org/10.1016/S0960-0779\(02\)00655-0](https://doi.org/10.1016/S0960-0779(02)00655-0), 2003. 1082  
1083  
1084
- Telesca, L., Lapenna, V., Vallianatos, F., Makris, J., and Saltas, V.: Multifractal features in short-term time dynamics of ULF geomagnetic field measured in Crete, Greece, *Chaos, Solitons and Fractals*, 21, 273–282, <https://doi.org/10.1016/j.chaos.2003.10.020>, 2004. 1085  
1086  
1087
- Telesca, L., Lapenna, V., and Macchiato, M.: Multifractal fluctuations in seismic interspike series, *Phys. A Stat. Mech. its Appl.*, 354, 629–640, 2005. 1088  
1089  
1090
- Turcotte, D. L.: Fractals in geology and geophysics, *Pure Appl. Geophys.*, 131, 171–196, 1989. 1091
- Turcotte, D. L.: Fractals and chaos in geology and geophysics, Cambridge university press, 1997. 1092
- Uyeda, S., Hayakawa, M., Nagao, T., Molchanov, O., Hattori, K., Orihara, Y., Gotoh, K., Akinaga, Y., and Tanaka, H.: Electric and magnetic phenomena observed before the volcano-seismic activity in 2000 in the 1093  
1094

- Izu Island Region, Japan, *Proc. Natl. Acad. Sci.*, 99, 7352–7355, 2002. 1095
- Virk, H. S., Walia, V., and Kumar, N.: Helium/radon precursory anomalies of Chamoli earthquake, Garhwal Himalaya, India, *J. Geodyn.*, 31, 201–210, 2001. 1096  
1097
- Wang, W., Cheng, Q., Tang, J., Pubuciren, Song, Y., Li, Y., and Liu, Z.: Fractal/multifractal analysis in support of mineral exploration in the Duolong mineral district, Tibet, China, *Geochemistry Explor. Environ. Anal.*, 17, 261–276, 2017. 1098  
1099  
1100
- Wendt, H.: Contributions of Wavelet Leaders and Bootstrap to Multifractal Analysis : Images , Estimation Performance , Dependence Structure and Vanishing Moments . Confidence Intervals and Hypothesis Tests, 1–292, 2008. 1101  
1102  
1103
- Werner, D. H., Haupt, R. L., and Werner, P. L.: Fractal antenna engineering: The theory and design of fractal antenna arrays, *IEEE Antennas Propag. Mag.*, 41, 37–58, 1999. 1104  
1105
- Weszka, J. S., Dyer, C. R., and Rosenfeld, A.: A comparative study of texture measures for terrain classification, *IEEE Trans. Syst. Man. Cybern.*, 269–285, 1976. 1106  
1107
- Xu, T., Moore, I. D., and Gallant, J. C.: Fractals, fractal dimensions and landscapes—a review, *Geomorphology*, 8, 245–262, 1993. 1108  
1109
- Xu, G., Han, P., Huang, Q., Hattori, K., Febriani, F., and Yamaguchi, H.: Anomalous behaviors of geomagnetic diurnal variations prior to the 2011 off the Pacific coast of Tohoku earthquake (Mw9.0), *J. Asian Earth Sci.*, 77, 59–65, <https://doi.org/10.1016/j.jseaes.2013.08.011>, 2013. 1110  
1111  
1112
- Yang, H., Pan, H., Wu, A., Luo, M., Konaté, A. A., and Meng, Q.: Application of well logs integration and wavelet transform to improve fracture zones detection in metamorphic rocks, *J. Pet. Sci. Eng.*, 157, 716–723, <https://doi.org/10.1016/j.petrol.2017.07.057>, 2017. 1113  
1114  
1115
- Yen, H.-Y., Chen, C.-H., Yeh, Y.-H., Liu, J.-Y., Lin, C.-R., and Tsai, Y.-B.: Geomagnetic fluctuations during the 1999 Chi-Chi earthquake in Taiwan, *Earth Planets Space*, 39–45 pp., 2004. 1116  
1117